

N° D'ORDRE: 3003

THESE EN CO-TUTELLE

FRANCE – THAILANDE

PRÉSENTÉE À

L'UNIVERSITE BORDEAUX 1
ECOLE DOCTORALE DES SCIENCES CHIMIQUES

ET

KASETSART UNIVERSITY
GRADUATE SCHOOL KASETSART UNIVERSITY

PAR TANIN NANOK

POUR OBTENIR LE GRADE DE

DOCTEUR

SPECIALITE: CHIMIE-PHYSIQUE

STRUCTURE ET DYNAMIQUE DE NANOMATÉRIAUX INDUSTRIELS

SOUTENUE LE: 14 JUILLET 2005

APRÈS AVIS DE:

PROF. MICHAEL PROBST, UNIVERSITÄT INNSBRUCK
PROF. YUTHANA TANTIRUNGROTECHAI, MAHIDOL UNIVERSITY BANGKOK

RAPPORTEUR
RAPPORTEUR

DEVANT LA COMMISSION D'EXAMEN FORMÉE DE:

PROF. BANCHA PANACHAROENSAWARD, KASETSART UNIVERSITY BANGKOK
PROF. JUMRAS LIMTRAKUL, KASETSART UNIVERSITY BANGKOK
PROF. PHILIPPE A. BOPP, UNIVERSITÉ BORDEAUX 1
PROF. ALEXANDER KUHN, UNIVERSITÉ BORDEAUX 1

PRÉSIDENT
EXAMINATEUR
EXAMINATEUR
EXAMINATEUR

MEMBRE INVITÉ:

DR. JEAN-CHRISTOPHE SOETENS, UNIVERSITÉ BORDEAUX 1

Deux méthodes hybrides issues de la chimie quantique ainsi que des simulations de dynamique moléculaire ont été utilisées pour étudier la structure, ainsi que les mécanismes d'adsorption, de réaction et de diffusion de molécules adsorbées dans des matériaux poreux industriels. Il a été démontré que le modèle d'agrégat intégré dérivé de SCREEP (Surface Charge Representation of Electrostatic Embedding Potential) prédit avec succès la surface d'énergie potentielle pour la réaction de protonation de l'éthylène dans la zéolite H-FAU. L'inclusion du potentiel électrostatique du réseau infini augmente l'énergie de liaison et, dû à l'abaissement de l'énergie d'activation, le degré de transfert de l'électron vers l'éthylène. Les énergies d'adsorption et d'activation calculées sont en bon accord avec les données expérimentales. Avec cette méthode on a pu non seulement prédire les profils énergétiques, mais aussi différencier la réactivité de différents types de zéolites. Afin de modéliser les effets de confinement sur le processus d'adsorption de molécules de tailles comparables à celles des pores, la méthode ONIOM (Our own N-layered Integrated molecular Orbital and molecular Mechanics), qui est basée sur un principe d'extrapolation, a été utilisée. La combinaison entre les différents niveaux de calcul (méthode de corrélation électronique et champs de force universel(UFF)) a été soigneusement calibrée et utilisée en vue de prédire les énergies d'adsorption des o-, m- et p-xylène dans la zéolite H-ZSM-5. Le domaine des énergies d'adsorption ainsi déterminées, 18-22 kcal/mol, est en bon accord avec les enthalpies d'adsorptions déduites de l'expérience.

Les études par simulation de la dynamique moléculaire du p-xylène dans la silicalite ont révélé que le processus de diffusion ressemble à un processus par sauts où la molécule diffusante résiderait pour des temps assez prolongés aux intersections des canaux avant de changer rapidement vers le site suivant. La vision microscopique corrobore l'observation expérimentale qu'à des taux de chargement supérieurs à quatre molécules par maille élémentaire les intersections et les canaux sinusoïdaux sont remplis simultanément alors que les canaux droits ne sont pas occupés. Afin de pouvoir étudier la diffusion dans le matériau mésoporeux MCM-41, un nouveau champ de force intermoléculaire a été développé. Les énergies d'adsorption obtenues avec ce nouveau champ de force sont associées pour l'essentiel avec les interactions van der Waals du modèle, alors que les contributions électrostatiques sont relativement faibles (de l'ordre de 2 kcal/mol). Pour tous les chargements étudiés, l'orientation des molécules de p-xylène adsorbées en première couche reste parallèle à la paroi.

ACKNOWLEDGEMENTS

I wish to express my deep gratitude to a number of people who giving me the guidance, help and support to reach my goal of this thesis. First of all, most of credits in this thesis should justifiably go to my advisors, Associate Professor Dr. Jumras Limtrakul and Professor Dr. Philippe Anthony Bopp, for their valuable guidance, continuous support, kindness and encouragement value assistance throughout the course of my graduate.

Furthermore, I would like to thank my committees, Professor Dr. Alexander Kuhn, Professor Dr. Michael Probst, Assistant Professor Dr. Yuthana Tantirungrotechai, Associate Professor Dr. Bancha Panacharoensaward, Assistant Professor Dr. Supa Hannongbua, and Dr. Pensri Boonsawansong who provided me for considerably helpful comments and discussion on various aspects to my work.

The Royal Golden Jubilee (RGJ) Ph. D. program and The French Embassy in Thailand are grateful acknowledged for financial support of my entire study. The Kasetsart University Research and Development Institute (KURDI) and the Ministry of University Affairs under the Science and Technology Higher Education Development Project (MUA-ADB funds) as well as the computational resources from Université Bordeaux I are also gratefully acknowledged for research support.

I am very grateful to my colleagues at Laboratory for Computational and Applied Chemistry (LCAC) at Kasetsart University for their providing considerably helpful assistance and encouragement during my study. A special thanks to Weerayuth Panyaburapa and Chompunuch Warakulwit for having helped me preparing the figures in many parts of this thesis.

In addition, all of my friends, my colleagues at Laboratoire de Physico-Chimie Moléculaire at Université Bordeaux I are also sincere thanked for their help and hospitality during my study in France.

Finally, I would like to express my most profound gratitude to my parents, my grandmother, my brothers and my sister, who sustained and encouraged me throughout the duration of my educations.

Tanin Nanok

July, 2005

TABLE OF CONTENTS

	Page
TABLE OF CONTENTS	i
LIST OF TABLES	iii
LIST OF FIGURES	v
LIST OF ABBREVIATIONS	vii
INTRODUCTION.....	1
LITERATURE REVIEW.....	5
MATERIALS AND METHODS.....	10
Methodologies.....	10
ONIOM (Our own N-layered Integrated molecular Orbital and molecular Mechanics).....	11
SCREEP (Surface Charge Representation of the Electrostatic Embedding Potential).....	15
Molecular Dynamics.....	20
Models and methods.....	25
Ethylene protonation reaction on H-FAU.....	25
Shape-selective adsorption of xylene isomers in H-ZSM-5.....	28
Diffusion mechanism of <i>p</i> -xylene in microporous silicalite.....	30
Silicalite structure.....	30
Potential parameters.....	31
Molecular dynamics simulations.....	35
Adsorption and diffusion of <i>p</i> -xylene in mesoporous MCM-41.....	36
Construction of the Si-MCM-41 structure.....	36
Potential parameters.....	37
Molecular dynamics simulations.....	39
RESULTS AND DISCUSSION.....	41
Charpter I: Ethylene protonation reaction on H-FAU.....	41
Brønsted active site.....	41
Adsorption complex.....	44

TABLE OF CONTENTS (cont'd)

	Page
Transition state.....	46
Surface alkoxide formation.....	49
Mechanistic aspects of the ethylene protonation on H-FAU.....	53
Chapter II: Shape-selective adsorption of xylene isomers in H-ZSM-5...	55
Adsorption structures.....	55
Adsorption energies.....	58
Chapter III: Diffusion mechanism of <i>p</i> -xylene in microporous silicalite..	60
Diffusion mechanism.....	60
Self-diffusion coefficients.....	63
Chapter IV: Adsorption and diffusion of <i>p</i> -xylene in mesoporous MCM-41.....	65
Structure and dynamics of empty Si-MCM-41, test of force field....	65
Adsorption of <i>p</i> -xylene.....	66
Self-diffusion of <i>p</i> -xylene.....	68
Radial distribution function.....	71
CONCLUSIONS.....	74
LITERATURE CITED.....	77
CURRICULUM VITAE.....	94

LIST OF TABLES

Table		Page
1	The different types of motion present in various systems together with suggested time steps.....	22
2	The potential parameters of silicalite zeolite	33
3	The potential parameters of xylene isomers.....	34
4	Partial charges of different atoms in <i>p</i> -xylene.....	34
5	The potential parameters of xylene-xylene and zeolite-xylene interaction.....	35
6	Potential parameters for short-range interactions between <i>p</i> -xylene and Si-MCM-41.....	39
7	Selected B3LYP/6-31G(d,p) parameters of active site of H-FAU zeolite calculated by using 3T, 5T and 7T cluster models. Bond lengths are in Å and bond angles in degrees. The values in the bracket are estimated by embedded cluster single point calculation.....	42
8	Selected B3LYP/6-31G(d,p) structural parameters and corrected adsorption energies (kcal/mol) of [C ₂ H ₄]/H-FAU complexes calculated by using 3T, 5T and 7T cluster models. Bond lengths are in Å and bond angles in degrees. The values in the bracket are estimated by embedded cluster single point calculation.....	45
9	Selected B3LYP/6-31G(d,p) structural parameters and corrected activation energies (kcal/mol) of [C ₂ H ₄]/H-FAU transition states calculated by using 3T, 5T and 7T cluster models. Bond lengths are in Å and bond angles in degrees. The values in the bracket are estimated by embedded cluster single point calculation.....	47

LIST OF TABLES (cont'd)

Table		Page
10	Selected B3LYP/6-31G(d,p) structural parameters corrected reaction energies (kcal/mol) of [C ₂ H ₄]/H-FAU surface ethoxides calculated by using 3T, 5T and 7T cluster models. Bond lengths are in Å and bond angles in degrees. The values in the bracket are estimated by embedded cluster single point calculation.....	51
11	Selected geometrical parameters and adsorption energies of <i>o</i> -, <i>m</i> -, and <i>p</i> -xylene adsorbed in H-ZSM-5.....	56
12	Self-Diffusion Coefficients (<i>D</i>) of <i>p</i> -xylene in silicalite at different loadings and temperatures.....	63
13	van der Waals, Coulomb, and total heats of adsorption energies and self-diffusion coefficients at different <i>p</i> -xylene loadings.....	67

LIST OF FIGURES

Figure		Page
1	The two-layer (left) and three-layer ONIOM extrapolation schemes	12
2	Different atom sets of the two-layer ONIOM scheme.....	13
3	Schematic diagram of the SCREEP embedded 7T cluster model.....	19
4	The flow chart of molecular dynamics simulation integrated by using the Verlet algorithm.....	24
5	Four different oxygen atoms in the FAU zeolite framework (top) and (a) 3T cluster, (b) 5T cluster, and 7T cluster models with Brønsted proton sitting on oxygen O1.....	27
6	The 184T cluster models viewing along straight channel (left) and zigzag channel (right); (a) the 5T/184T ONIOM(MP2/6-31G(d,p):UFF) and (b) the 5T/23T/184T ONIOM(MP2/6-31G(d,p) : B3LYP/631G(d,p):UFF).....	28
7	The optimized adsorption structure of (a) <i>o</i> -, (b) <i>m</i> -, and (c) <i>p</i> -xylene in the intersecting channel of H-ZSM-5 viewing along straight channel (left) and zigzag channel (right).....	29
8	Model of Si-MCM-41; the hexagonal lattice framework (left) and the Si-MCM-41 supercell (right).....	37
9	The optimized adsorption structures of ethylene on H-FAU using (a) 3T, (b) 5T, and (c) 7T cluster models.....	43
10	The optimized structures of ethylene protonation transition state using (a) 3T, (b) 5T, and (c) 7T cluster models	48
11	The optimized structures of surface ethoxide using (a) 3T, (b) 5T, (c) 7T cluster models.....	52
12	The adsorption complex of (a) <i>o</i> -xylene, (b) <i>m</i> -xylene, and (c) <i>p</i> -xylene in the intersecting channel of H-ZSM-5. The extended framework is omitted for clarity.....	57

LIST OF FIGURES (cont'd)

Figure		Page
13	Guest molecule trajectories during 1 ns, from a simulation with a loading of 1 p-xylene per unit cell at a temperature of 500 K. The trajectory is projected onto the xy (a) and xz (b) planes.....	61
14	Molecular positions and orientations of p-xylene (a) before the jump and (b) during the jump in the channels of silicalite at a loading of 4 molecules per unit cell (500 K).....	62
15	Simulated IR spectrum of the model Si-MCM-41.....	66
16	Mean square displacements (MSDs), at 300 K, of the centers of mass of the p-xylene molecules in Si-MCM-41 at different loadings.....	68
17	The normalized autocorrelation functions at 300 K of the velocity of the mass centers of the p-xylene molecules in Si-MCM-41 at different loadings.....	69
18	Projections of the trajectories of the centers of mass of p-xylene and the framework atoms (for 100 ps) onto the xy-plane at a loading of 16 molecules/supercell (black clouds and dots); cylindrical g(r) distribution function of the p-xylene centers of mass with respect to the center of the channel for this and other loadings.....	70
19	Snapshots of the distribution of p-xylene molecules in Si-MCM-41 supercell at loading of (a) 16, (b) 32, (c) 48, and (c) 64 molecules per supercell after 100 ps of MD equilibrium.....	71
20	The center-center pair distribution functions of p-xylene in Si-MCM-41 at different loadings.....	72
21	Illustration of (a) the configuration of p-xylene dimer optimized at B3LYP/6-31G(d,p) level of theory (b) a snapshot of p-xylene molecules in the center channel of Si-MCM-41 supercell at loading of 64 molecules per supercell after 100 ps of MD equilibrium.....	73

LIST OF ABBREVIATIONS

B3LYP	=	Becke's three parameter hybrid functional using the LYP correlation functional
BSSE	=	Basis Set Superposition Error
GVFF	=	Generalized Valence Force Field
HF	=	Hartree Fock
K	=	Kelvin
kcal/mol	=	kilocalorie per mol
LJ	=	Lennard-Jones
MD	=	Molecular Dynamics
MP2	=	the second-order Møller-Plesset perturbation theory
MSD	=	Mean Square Displacement
ONIOM	=	Our own N-layered Integrated molecular Orbital and molecular Mechanics
QM/MM	=	Quantum Mechanics and Molecular Mechanics
SCREEP	=	Surface Charge Representation of Electrostatic Embedding Potential
T	=	Tetrahedral
UFF	=	Universal Force Field

STRUCTURE AND DYNAMICS OF INDUSTRIAL NANOMATERIALS

INTRODUCTION

Zeolites are three-dimensional, microporous, crystalline solid with well-defined structures. Compositionally, their regular framework contains aluminium and silicon atoms that are tetrahedrally coordinated with each other through shared oxygen atoms. The presence of aluminium atoms in the framework causes a number of residual negative charges on the oxygen framework. These negative charges are normally compensated by the cations which can easily be exchanged by other cations. The ion-exchange property of zeolites, which allows the replacement of cations held in their cages or channels by ions present in the external solutions, has been intensively studied and widely used in industry for a wide range of applications including adsorption and separation of gases and hydrocarbons, catalysis, drying, etc. (Bekkum *et al.*, 1991; Ruthven, 1984).

A protonic form of zeolites can be generated by exchanging the nonframework metal cations (M^+) with ammonium or alkylammonium ions followed by calcination. This form of zeolites is able to transfer a proton from the zeolite surface to the adsorbed molecule. Thus, this type of active center is called a Brønsted acid site. The acid strength can be determined by microcalorimetry and IR spectroscopy of small adsorbed probe molecules such as CO, H₂ or ethylene (Dwyer, 1991; Trombetta *et al.*, 2000). By using microcalorimetric method, the quantitative data of the adsorption heat and the number of acid sites are obtained. IR spectroscopy is used to examine either the nature of the OH bond by observing the OH stretching frequency of different zeolites or the characteristic frequencies of probe molecules interacting with Brønsted acid sites.

When discussing the zeolite acidity, the information of the interaction of probe molecules with the acid sites obtained by theoretical calculations has become increasingly important. However, the results derived by using small cluster model to

represent the zeolite active sites are still not in good agreement with the experimental results. Furthermore, the use of an unconstrained small cluster model is not able to represent any types of zeolites. The attempt to include the effects of extended framework, especially the electrostatic Madelung potential, has been made by many research groups (Allouche, 1996a, b; Ferrari and Pacchioni, 1996; Ferro *et al.*, 1995). Periodic density functional theory calculations by using the plane wave basis set was found to give quite encouraging results in describing the interaction between small polar molecules with the acid sites (Boronat *et al.*, 1999; Boronat *et al.*, 2001a; Larin *et al.*, 2005; Schwarz *et al.*, 1997; Shah *et al.*, 1996; Shah *et al.*, 1997). This approach, however, is limited to only the small unit cell zeolites such as chabazite (36 atoms) (Boronat *et al.*, 1999; Brandle *et al.*, 1998; Rozanska *et al.*, 2002a), ferrierite (108 atoms) (Mickael *et al.*, 2003) or mordenite (144 atoms) (Rozanska *et al.*, 2002b; Rozanska *et al.*, 2001, 2002c; Vos *et al.*, 2001) due to the expensive computational demand. For commercially important zeolites like ZSM-5 and FAU, which contains 288 and 576 atoms per unit cell respectively, the applications of this methodology are still impractical. The hybrid quantum mechanics/molecular mechanics (QM/MM) is a method of choice widely used to model condensed phase structure and reactivity (Clark *et al.*, 2002; Joshi and Thomson, 2005; Martinez-Magadan *et al.*, 2002; Shor *et al.*, 2005). In these methods, the active region can be treated with high accurate quantum calculations while the effects of surrounding environment on the active region are described by the force fields. Accordingly, the interaction between the active region and its environment can be represented exclusively by molecular mechanics. This is referred to as “mechanical embedding” in which the environment of the QM system has no direct effect on the electron distribution within the QM system (Svensson *et al.*, 1996). However, if the molecular mechanics Hamiltonian contains a description of Coulomb interactions, then it is possible to incorporate these interactions into the quantum mechanical Hamiltonian. As a result, one can account for the polarization of the electron distribution within the QM system in the present of the electrostatic potential of its environment. In this case, it is referred to as “electronic embedding” (Stefanovich and Truong, 1998).

In this study, the acidity and reactivity of H-FAU zeolite were examined by using the description of the interaction between the probe molecule and Brønsted acid site. Ethylene, the smallest unsaturated hydrocarbon and the precursor of valuable aromatic hydrocarbons, was chosen as the adsorbed probe molecule. Both bare cluster and embedded cluster models were used to describe the local active site of these zeolites. For the embedded cluster models, the electrostatic contribution from extended framework was taken into account by using the electronic embedding approach according to the SCREEP (surface charge representation of the electrostatic embedding potential) formalism (Stefanovich and Truong, 1998). The effects of cluster size on the acidity and potential energy surface of the ethylene protonation reaction were also discussed.

Shape-selective separation and catalysis are of the most important characteristics of zeolites utilized in petrochemical industry. These properties are based on restricted molecular adsorption and diffusion in the microporous network, in which only molecules of a size comparable to or smaller than the pore openings are able to be selectively taken up into their micropore structure while the others are rejected. FAU and ZSM-5 are widespread used for these purposes, especially in the separation of *p*-xylene from C8 aromatics (*p*-, *o*-, *m*-xylene and ethylbenzene), which is a vital step in the large scale synthesis of petrochemicals (Bellat *et al.*, 1997; Bellat and Simonot-Grange, 1995a; Bellat *et al.*, 1995b; Guo *et al.*, 2000; Mohanty *et al.*, 2000; Namba *et al.*, 1997; Niessen and Karge, 1993; Sakai *et al.*, 2001). This isomer is the most interesting; it is at the basis of the production of polyester films and fibers. In order to better understand the shape-selective property of ZSM-5 zeolite in the separation of *p*-xylene from other xylene isomers, the adsorption process of three xylene isomers (*p*-, *o*-, and *m*-xylene) on H-ZSM-5 was studied. Since xylenes are non-polar molecules, the long-range electrostatic contributions are not expected to be significant. The mechanical embedding scheme known as ONIOM (Our-own N-layered Integrated molecular Orbital and molecular Mechanics) method is, thus, more appropriate for this purpose (Svensson *et al.*, 1996). By combining different levels of calculation, this approach has an advantage over the SCREEP method in that the

mechanical confinement effects in zeolites can be investigated with reasonable computational cost.

In addition to the adsorption property, the details of diffusive processes of molecules adsorbed in the micropores of zeolites and the influence of the framework structure and dynamics on diffusion would be very useful to understand the zeolite behavior and facilitate the selection of zeolites for a specific application. Consequently, the diffusion mechanisms of *p*-xylene in silicalite (aluminium-free ZSM-5) and in mesoporous MCM-41 were simulated. Molecular dynamics (MD) simulations are a choice technique to approach this phenomenon.

LITERATURE REVIEW

Zeolites are important catalysts for many industrial processes, due mainly to their shape- and size-selectivity. Reactions of hydrocarbon compounds on zeolites have been widely studied, especially in hydrocarbon transformation which is a major process of many practical important in the field of oil refining, petrochemical industry and fine chemical productions. Acidic zeolites, which have a Brønsted proton sitting on bridging oxygen atom, are strikingly active for catalyzing reactions of hydrocarbons such as hydrocarbon cracking (Blaszkowski *et al.*, 1996; Corma and Orchilles, 2000; Frash *et al.*, 1998), polymerization (Vaya *et al.*, 2001), aromatization (Choudhary *et al.*, 2001; Choudhary *et al.*, 2002; Ha *et al.*, 2002), and isomerization reactions (Ivanov and Papp, 2000).

One of the zeolite-catalyzed hydrocarbon reactions of industrial interest is the protonation reaction of unsaturated hydrocarbons in acidic zeolites (Kazansky, 2002; Kondo *et al.*, 1998). It has been found that such process occurs through a concerted mechanism: the proton transfer from zeolite to a carbon atom of unsaturated hydrocarbon occurs simultaneously with the C-O bond formation at the adjacent bridging oxygen on the zeolite framework (Boronat *et al.*, 1998; Correa and Mota, 2002; Kazansky, 1999; Viruela-Martin *et al.*, 1993). The protonation reaction of ethylene in zeolites, which is a prior step of such reactions above, is one of the most important key steps in zeolite science and engineering. Theoretical studies using accurate quantum mechanical methods can provide, in addition to the energetic properties, details on the adsorption structure. Previous theoretical studies proposed that the protonation reaction mechanism of ethylene within acidic zeolite occurs via ionic- like transition state followed the covalent bond formation of a stable ethoxy intermediate (Evleth *et al.*, 1996; Kazanskii, 1991b; O'Malley and Farnworth, 1998; Ugliengo *et al.*, 1996). All of these studies, however, used small gas phase cluster models in an unconstrained environment, such as $\text{HOAlH}_2\text{OH}_2$, $\text{HOAl}(\text{OH})_2\text{OH}_2$, and $\text{H}_3\text{SiOAlH}_2\text{OHSiH}_3$, to represent the active sites of zeolites, hence neglecting the effects of zeolite framework, particularly the long-range electrostatic effect caused by

the Madelung potential from the zeolite lattice (Boronat *et al.*, 1999; Zygmunt *et al.*, 2000). The predicted adsorption energy of ethylene (-4 to -7 kcal/mol) (so far are noticeably smaller compared to the experimental adsorption energy of ethylene on the acidic H-Y zeolite (-9 kcal/mol) (Cant and Hall, 1972). Such deviation indicates that the effects of extended zeolite framework could be an important factor in stabilizing the adsorption complex. In this aspect, the periodic electronic structure calculation can be employed (Barbosa *et al.*, 2001; Boronat *et al.*, 2001b; Rozanska *et al.*, 2002a; Rozanska *et al.*, 2002b). The zeolitic host system is represented by an infinite crystal. However, the computational cost of periodic calculations depends on both the symmetry and the unit cell size of zeolite. Normally, only systems with high symmetry and small unit cell can be evaluated. It is, therefore, not practical to apply this periodic calculation to the commercial zeolites, which usually have large unit cells.

With the comparable accuracy and the relatively low computational cost compared with periodic calculation, the electronic embedded cluster methodology is an alternative way to be used (Stefanovich and Truong, 1998). By the classical formalism of this methodology, the cluster enclosed by a set of point charges can be calculated with high level quantum chemical calculation methods. The applications of these methods have been addressed in many publications (Limtrakul *et al.*, 2000a; Limtrakul *et al.*, 2000b; Limtrakul *et al.*, 2001; Treesukol *et al.*, 2001a; Vollmer *et al.*, 1999; Vollmer and Truong, 2000). In our previous work, the inclusion of Madelung potential represented by a finite number of point charges derived by SCREEP method was found to have a dramatic effect on the adsorption energies of ethylene on protonated zeolites (Limtrakul *et al.*, 2001). This approach not only discriminates against the acidity of H-FAU and H-ZSM-5 but also provides a good agreement with the experiment for the adsorption energy of ethylene on H-FAU. Therefore, it is expected that the Madelung potential of the extended zeolite lattice should affect the potential energy surface and, hence the reaction mechanism.

In addition to the improvement of energetic properties, the detailed structures of intermediates generated along the reaction path are also needed to be corrected. The model used to represent the local active site should include all short-range interactions that might play a dominant role in determining the optimized geometry. Although the large cluster model takes into account all important parts of the active region, it requires much computational demand. Therefore, the optimal cluster size is thus necessary to be selected in order to compromise between the cost efficiency and accuracy.

Size and shape selective separations of xylene isomers using zeolites are of industrial interest topics. In particular, silicalite membranes have received a great deal of attention in recent years with the aim to reduce the very energy-intensive separation process of *p*-xylene from other isomers (Mohanty and McCormick, 1999). The adsorption and transport of xylene isomers, and in particular of *p*-xylene, has been quite extensively studied experimentally (Ashtekar *et al.*, 2000). The isosteric heat of adsorption observed for *p*-xylene loadings greater than 4 molecules per unit cell was ~80 kJ/mol (~19 kcal/mol), and the differential molar entropy of adsorption indicated an increase in ordering of the sorbed phase with increasing coverage (Richards and Rees, 1988). X-ray diffraction data revealed that *p*-xylene is located at the channel intersection with its long molecule axis nearly parallel to the straight channel (Mentzen and Gelin, 1998) while *o*- and *m*- xylene are located near the channel intersection with the methyl groups oriented approximately into the straight and sinusoidal channels (Nair and Tsapatsis, 2000). The diffusion studies reported that *p*-xylene penetrates freely and rapidly in ZSM-5/silicate in contrast to *o*- and *m*-xylene that penetrate only slowly (Niessen *et al.*, 1993; Roque-Malherbe *et al.*, 1995). This behavior can often be generally understood in terms of the size of the sorbate molecules relative to the channel systems. Although extensive investigation of zeolite beds and membranes has been explored, many aspects of size and shape selective separations using zeolites are not yet well understood. Intensive study of adsorption and diffusion process of different xylene isomers in zeolite pores would help to better understand the general principles of shape selective separation.

Recently, quantum mechanical calculation based on the combination of different levels of calculation known as ONIOM method has been proven as a powerful to tackle the adsorption problems. This method was successfully applied for modeling the confinement effect of zeolite lattice on the adsorption process of aromatic hydrocarbons (Namuangruk *et al.*, 2004; Raksakoon and Limtrakul, 2003). The adsorption energy was found not only depending on the local active site but also on the zeolite framework. With respect to the zeolite confinement, the adsorbed molecules can adopt their orientations to the most energetically preferable configuration.

It should be emphasized that the diffusion process is the most important step to understanding the shape selective catalysis: the sorbate molecules have to penetrate through the channel systems before any reaction takes place at the active site. However, diffusion processes are very difficult to characterize at microscopic level by experiment since all kinds of artifacts like impurities, defect etc. may interfere with the measurement and render the interpretation difficult. Molecular dynamics simulations are choice technique to solve this problem: they have been verified to be effective in exploring the microscopic mobility and diffusion in several guest molecule(s)/zeolite systems (Karger *et al.*, 2003). This approach, of course, does not include any chemisorption phenomena, which usually requires quantum chemical calculations. In tight-fitting systems like the one discussed here, the coupling between the motion of the guest molecules and of the zeolite itself can be expected to be important. However, only few flexible-lattice simulations have been carried out concerning the diffusion of xylene (Sastre *et al.*, 1998). This may be due to high demand in terms of computational time.

Unlike zeolites, MCM-41 is novel mesoporous material, which has a large surface area and adsorption capacity (Beck *et al.*, 1992). It can be synthesized in its high-silica form (Si-MCM-41) and also in its high-alumina form (Al-MCM-41). The high-silica form of MCM-41 is structurally stable to thermal and hydrothermal treatment. It has, therefore, great potential for practical use as an adsorbent and

mesoporous support for depositing active catalysts (Girgis and Tsao, 1996). Its large pore diameter with fewer diffusional constraints can deactivate coke formation due to the building up of bulky products not able to diffuse out. In addition, this material also permits the simultaneous entry of several reactant molecules into the pores, thus yielding high conversion (Climent *et al.*, 1996; Katada *et al.*, 1995). Although the reactivity of MCM-41 has been extensively investigated experimentally (Zhao *et al.*, 1996), relatively few theoretical studies have been reported (Cao *et al.*, 2004; Feuston and Higgins, 1992; Kleestorfer *et al.*, 2001; Maddox *et al.*, 1997; Ravikovitch *et al.*, 1995; Ravikovitch *et al.*, 1997; Sonwane and Li, 2005). This might be due to the large number of atoms necessary to describe the MCM-41 structure without applying restrictive symmetry constraints. Furthermore, complete structural information at the atomic level is still not available.

Research on adsorption and diffusion of aromatics in MCM-41 is of particular interest since many separation processes and reactions of industrial interest in MCM-41 are concerned with bulky aromatic compounds. However, only a few adsorption isotherms of aromatic hydrocarbons in MCM-41 have been determined experimentally. Benzene, toluene, *p*-xylene, mesitylene, and naphthalene have nevertheless been investigated over a wide range of temperatures (Choudhary and Mantri, 1998; Choudhary and Mantri, 2000b; Nguyen *et al.*, 1998). Understanding the adsorption and diffusion mechanism will be helpful for the interpretation of other reactions in this material. These phenomena can be observed experimentally by a variety of methods, mostly spectroscopic, which are, however, often particularly difficult in porous materials. Furthermore, it is usually not possible to derive a consistent microscopic picture of the diffusion process, or processes, only from the experiments.

MATERIALS AND METHODS

Methodologies

In the embedded quantum mechanical calculations, only a small active part of the crystal lattice is treated by approximately accurate quantum mechanical methods. This quantum mechanical region is referred to as the cluster. The rest of the crystal will be called the environment, which is usually represented by a less accurate method of calculation. The action of the environment on the quantum cluster can be classified into two crucial aspects. First, the environment has no direct effect on the electron distribution within the quantum cluster. The interaction between quantum cluster and its environment is described exclusively by molecular mechanics. This is noted as “mechanical embedding”, which means that there is a trivial effect as far as changes in electron distribution with geometry are concerned. The environment can be modeled by either a force field or a computationally less expensive quantum mechanical method. The former is known as a hybrid quantum mechanics and molecular mechanics (QM/MM) method (Deka and Hirao, 2002; Hillier, 1999; Joshi *et al.*, 2005; Sherwood *et al.*, 2003) and the latter is recognized as the more general ONIOM (our own N-layered molecular orbital and molecular mechanics) scheme (Svensson *et al.*, 1996). Applications of the ONIOM methodology to study the reactions in zeolites have recently been reported (Bobuatong and Limtrakul, 2003; Jiang *et al.*, 2005; Kasuriya *et al.*, 2003; Namuangruk *et al.*, 2004; Panjan and Limtrakul, 2003; Raksakoon *et al.*, 2003; Rungsisakun *et al.*, 2004; Sillar and Burk, 2004). Second, if the environment contains electric charges, it is possible to transfer the resulting Coulomb interactions into the quantum mechanical Hamiltonian of the cluster. In this way, one can account for the polarization of the electron distribution within the quantum cluster. In this case, the so-called “electronic embedding”, the force field parameters, such as point charges, would have to provide a reasonably accurate representation of the environmental electrostatic potential. One of the methods that have been proven to be very promising for the treatment of long-range electrostatic potentials of the extended system is the SCREEP (surface charge

representation of the electrostatic embedding potential) method (Stefanovich and Truong, 1998). The accuracy of this method for modeling adsorption processes in zeolites has already been addressed in several previous studies (Ketrat and Limtrakul, 2003; Limtrakul *et al.*, 2000a; Limtrakul *et al.*, 2000b; Rungsirisakun *et al.*, 2004; Treesukol *et al.*, 2001a; Treesukol *et al.*, 2001b).

In this thesis, an ONIOM scheme was used to model the effect of the confinement on the adsorption processes of *o*-, *m*-, and *p*-xylene in H-ZSM-5 while the SCREEP method was applied to investigate the influence of the electrostatic Madelung potential of the extended framework on the adsorption and protonation of ethylene in H-FAU zeolite. Since it is important to understand the theory background of these methods in order to assess the reliability of the results, they should be discussed in some details in the following sections.

1. ONIOM (our own N-layered integrated molecular orbital and molecular mechanics)

The ONIOM method was first developed by Svensson *et al.* (1996) on the basic idea of partitioning the system into two or more different parts or layers to approximate the entire system calculated at the highest possible level of theory. The region of the system where the chemical process takes place, for example bond breaking and formation, is treated with a high level quantum mechanical method, while the remainder of the system is treated at a lower level. Each layer can, in principle, be treated at an arbitrary level of theory. The two-layer and three-layer ONIOM extrapolation schemes are shown in Figure 1.

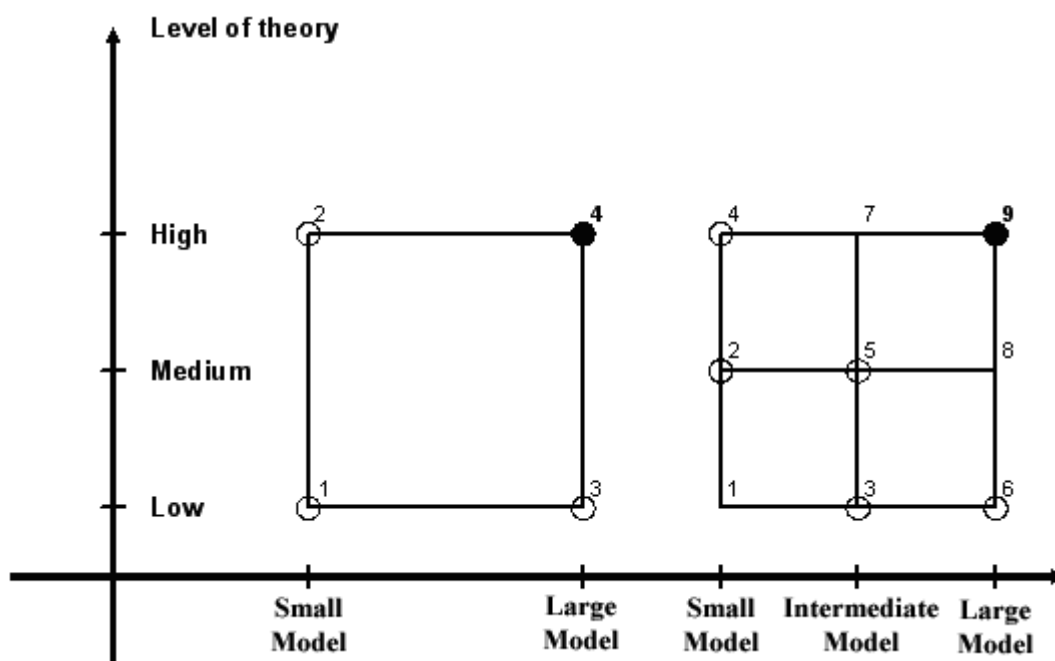


Figure 1 The two-layer (left) and three-layer ONIOM extrapolation schemes.

In the two-layer ONIOM calculation, the extrapolated total energy of the system is obtained from three independent calculations:

$$E_{\text{ONIOM}_2} = E_3 - E_1 + E_2 \quad (1)$$

where E_3 is the energy of the large (real) system calculated only at a low level method and E_1 and E_2 are the energies of a small model system determined at the low and high level of theory, respectively. E_{ONIOM_2} is an approximation of the total energy of the large system at high level E_4 :

$$E_4 = E_{\text{ONIOM}_2} + D \quad (2)$$

Therefore, if the error D of the procedure is constant for two different structures (e.g. between reactant and transition state), their relative energy ΔE_4 will be evaluated correctly by using the ONIOM energy $\Delta E_{\text{ONIOM}_2}$.

For a system partitioned into three different layers, the expression for the total energy E_{ONIOM3} , as an approximation for E_9 , can be defined as:

$$E_{ONIOM3} = E_6 - E_3 + E_5 - E_2 + E_4 \quad (3)$$

An important and critical feature of all the combination schemes is the treatment of the boundary region between different levels of calculation. If there is no covalent bond between layers, there is no special boundary region. However, if an accurate description of a particular region of a large organic molecule or a macromolecule is required, some covalent bonds at the boundary region have to be cut in order to generate the inner model system. This process leaves dangling bonds at the border of the inner layer, which have to be saturated, usually with hydrogen atoms, in order to avoid a chemically unrealistic model. These hydrogen atoms are so-called link atoms and are only present in the model system.

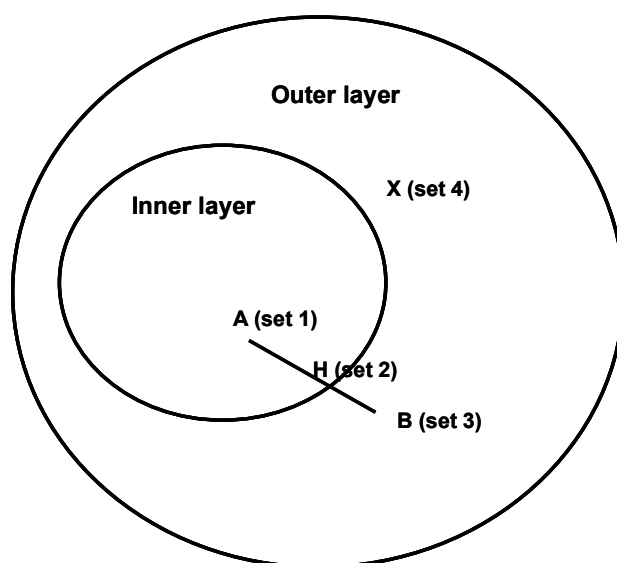


Figure 2 Different atom sets of the two-layer ONIOM scheme.

Figure 2 illustrates the definition of different atom sets within the two-layer ONIOM scheme. The set 1 atoms, belonging to the inner layer, are a constituent element of the model system and their coordinates are denoted by R_I . The set 2 atoms

are the artificially introduced link atoms and their coordinates are described by R_2 . In the large system, these atoms are replaced by the set 3 atoms with the coordinates R_3 . Atoms that belong to the outer layer and are not substituted by link atoms are called set 4 atoms and their coordinates are specified by R_4 .

Because the link atoms are introduced to mimic the corresponding covalent bonds of the large system, they should follow the movement of the atoms they replace. In the model calculations, these link atoms are always aligned along the bond vectors of the large system. Therefore, their coordinates R_2 are defined as a function of the coupling between R_1 and R_3 :

$$R_2 = f(R_1, R_3) \quad (4)$$

If atom A belongs to set 1 and atom B belong to set 3, the set 2 link atom (symbolized by H in Figure 2) is placed onto the bond axis A-B. To address the exact position r_2 of a link atom (H) along an A-B bond ($r_3 - r_1$), the distance parameter g is introduced. Hence

$$r_2 = r_1 + g(r_3 - r_1) \quad (5)$$

From this relationship, if the A-B bond distance $|r_3 - r_1|$ changes during a geometry optimization, the A-H bond distance $|r_3 - r_1|$ also changes. In this study, to generate the zeolite model system, the boundary Si-O bonds are substituted by Si-H bonds. A selected reasonable value for g is 0.8802, which is a standard Si-H bond length (1.47 Å) divided by a standard Si-O bond length (1.67 Å).

Once an expression of the two-layer ONIOM energy along with a certain functional relationship between set 2 and set 1/3 atoms (equation 1 and 5) has been defined, the definition of the corresponding integrated gradient expression is straightforward.

$$\nabla E_{\text{ONIOM2}} = \nabla E_3 - \nabla E_1 \cdot J(R_2; R_1, R_3) + \nabla E_2 \cdot J(R_2; R_1, R_3) \quad (6)$$

where J , the Jacobian matrix, projects the forces on all the set 2 link atoms (R_2) onto the set 1 (R_1) and set 3 atoms (R_3). The differentiation of the vector components of one set 2 atom r_2 with respect to the components of r_1 and r_3 yields a very simple Jacobian:

$$\partial r_{2,a} / \partial r_{3,b} = g \delta_{a,b} \quad (7)$$

$$\partial r_{2,a} / \partial r_{1,b} = (1-g) \delta_{a,b} \quad (8)$$

where the indices a and b denote the Cartesian components x , y and z , and δ is the Kronecker symbol. It should be emphasized that this particular coupling scheme allows a rigorous and consistent definition of the energy derivatives without complicated transformation. The methodology in case of a three-layer ONIOM is exactly the same and will not be discussed explicitly.

2. SCREEP (Surface Charge Representation of the Electrostatic Embedding Potential)

In the SCREEP method, the action of the environment on electrons in the quantum cluster is exclusively represented by the electrostatic, or Madelung, potential $V_{el}(r)$ (Stefanovich and Truong, 1998). The infinite lattice electrostatic potential is modeled by a finite number of point charges placed outside the cluster. This approach allows to calculate analytically the matrix elements related to the point-charge potential as well as their first and second derivatives. This is implemented in most quantum chemistry programs. The accuracy of such a method critically depends on the selection of the total number of point charges, their positions r_i , and values q_i . The determination of the SCREEP charge values q_i can be carried out in three steps:

1. Construct and discretize the closed SCREEP surface around a cluster: this determines the number of point charges and the positions.

2. Calculate the Madelung potential $V_{el}(r)$ resulting from the real distribution of the charges replaced outside the surface on the surface elements.
3. Solve linear equations to obtain the charge values q_i associated with each element of the SCREEP surface.

Conventionally, the SCREEP surface S around a cluster was built and discretized as “van der Waals” surfaces from atomic spheres of a fixed radius R_a (2.5-3.0 Å). To apply this method in zeolites, in this study, the surface S was built as a sphere of a fixed radius R_s from the zeolite cavity center. The radius of this spherical surface was set to the value that enables to enclose the entire van der Waals surface of the quantum cluster atoms. This surface was divided into M surface elements with areas S_i . The point charges q_i will be positioned at the center of the surface elements r_i .

In order to determine the magnitude surface charges, the electrostatic potential $V_{el}(r)$ generated by charge distribution outside of the surface S was projected onto the center of the surface elements by using the Ewald technique. The matrix elements of the electrostatic potential at all points r_i on the surface were then used to derive the charge values by using a matrix equation:

$$V_{el}(r_i) = A_{ij}q_i \quad (9)$$

where $V_{el}(r_i)$ is the value of the external electrostatic potential at point r_i and A_{ij} is the nonsingular matrix with matrix elements:

$$A_{ij} = \frac{1}{|r_i - r_j|} \quad \text{for } i \neq j \text{ and } A_{ii} = \sqrt{1.07(4\pi/S_i)} \quad (10)$$

The nondiagonal elements A_{ij} represent a generic Coulomb interaction between surface elements r_i and r_j . The diagonal elements A_{ii} represent the self-interaction of the surface element r_i . The coefficient 1.07 was fitted for better

numerical accuracy (Klamt and Schuurmann, 1993). The values of the surface charges q_i can be determined by applying any technique available for solving systems of linear equations. One can use the matrix inversion method:

$$q_i = A_{ij}^{-1} V_{el}(r_i) \quad (11)$$

According to the conducting boundary condition (Stefanovich and Truong, 1998) used in this technique, the electrostatic potential generated by the charge density $\sigma(r_i)$, which is now represented by M point charges q_i , on the surface S , is exactly equal to the original potential $V_{el}(r_i)$. Therefore, the external electrostatic potential inside the surface S can be reproduced by these point charges located on the surface S .

The accuracy can be improved if ions from the environment that are close to the quantum cluster and the surface S are treated explicitly without the SCREEP approximation; i.e., their potential is directly evaluated inside the cluster and not taken into account in equation 9. The simplest way to specify the explicitly treated region of the environment is by selecting a cutoff radius R_{cut} ($R_{cut} > R_s$). Then all lattice ions in the environment lying within R_{cut} to the closest atom of the cluster are attributed to the explicit region.

Therefore, the SCREEP embedded cluster model used in this study consists of three layers, as shown in Figure 3. The center layer is the quantum chemical cluster. The next layer of the model is a set of explicit point charges derived from periodic population analysis on zeolite systems. These point charges were placed at the atomic centers of the zeolite framework obtained from X-ray crystallographic data. To minimize the errors due to the interactions that occur between the quantum mechanical terminating hydrogens and the neighboring point charges, the layer of explicit point charges nearest to the quantum cluster was moved out. By this way, the values of point charges in the next layer were readjusted, by fitting to minimize deviations from the original external electrostatic field. The outermost layer of the

model is the SCREEP surface, which is represented by finite number of surface point charges to represent the remaining Madelung potential from the extended zeolite crystal. The schematic diagram of the SCREEP model used in this study is shown in Figure 3.

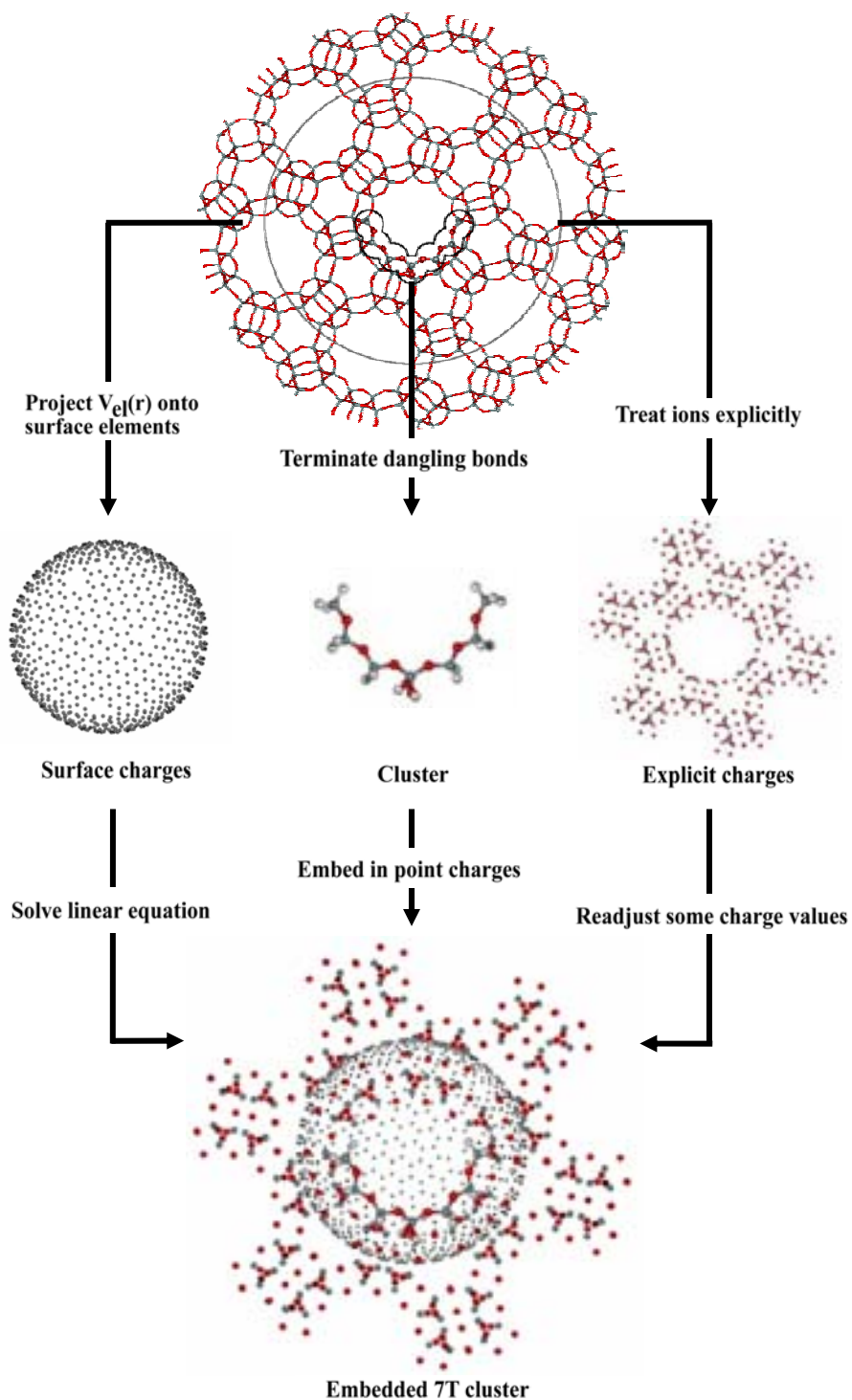


Figure 3 Schematic diagram of the SCREEP embedded 7T cluster model.

3. Molecular Dynamics

Molecular dynamics (MD) is a method for studying the microscopic behavior of well-defined systems of interacting particles through the solution of the classical equations of motion. This technique was invented in 1957 by Alder and Wainwright in order to investigate the phase behavior and transport properties in the hard sphere gas (Alder and Wainwright, 1957). It has been applied to a wide range of problems in condensed matter physics. The application of the MD technique to zeolites has increasingly attracted the attention of several research groups, especially in the topics of the molecular sieving and transport properties (Kärger *et al.*, 2003).

In molecular modeling, the Born-Oppenheimer approximation is invariably used to treat electrons separately from the nuclei. This approximation is based on the fact that the mass of each electron is much less than that of the nuclei. Consequently, the wave function of the system can be separated into an electronic contribution and a contribution from the nuclei.

$$\Psi_{total}(nuclei, electron) = \Psi(electron) \cdot \Psi(nuclei) \quad (12)$$

For each set of nuclear positions, the electronic Schrödinger equation can be solved to get the energy contributed by electrons. This energy along with the nuclear-nuclear repulsions then determines the total potential energy, and can be used to find the forces on the atoms. This energy, which is now a function of atomic positions only, is called a potential energy surface and can be approximated by an analytic function that gives the potential energy and interatomic forces as a function of coordinates. The latter is called a potential energy function.

In molecular dynamics, given a potential energy function $U(r_1, \dots, r_N)$ for a system of N interacting particles, successive configurations of the system are generated by integrating Newton's laws of motion.

$$F_i = m_i a_i = \frac{d^2 r_i}{dt^2} \quad (13)$$

where F_i is the force on particle i due to its interactions with other particles, m_i is the mass of particle i , and a_i is the acceleration of particle i . The force is determined from the potential energy function, which is a sum of pair potentials.

$$U(r_1, \dots, r_n) = \sum_{i,j} u(r_{ij}) \quad (14)$$

where r_{ij} is the separation between particle i and j . The force F_i acting on particle i is then:

$$F_i = -\frac{\partial U}{\partial r_i} = \sum_{j \neq i} f_{ij} \quad (15)$$

Here the f_{ij} is the force on particle i due to its interaction with particle j :

$$f_{ij} = -\frac{\partial u(r_{ij})}{\partial r_{ij}} \quad (16)$$

Under the influence of the interaction potential, the motions of all the particles are coupled together, giving rise to a many-body problem that cannot be solved analytically. In such circumstances, the equations of motions are integrated by using a finite difference method that can be solved iteratively. To generate molecular dynamics trajectories, the integration is broken down into many small stages, each separated in time by a fixed time δt . The total forces on the particles in the configuration at a time t is used to determine their accelerations, which are then combined with the positions and velocities at a time t to calculate the positions and velocities at time $t + \delta t$. The forces on the particles in their new positions are then determined, leading to new positions and velocities at time $t + 2\delta t$, and so on.

There are many algorithms for integrating the equations of motion using finite difference methods. Various factors may need to be taken into account when deciding which is most appropriate. The most important circumstances are that the integration algorithm should conserve energy and momentum, be time reversible, and should permit a long time step, δt , to be used. The size of the time step is particularly relevant to the computational demands. A simulation using a long time step will require fewer iterations to cover a given amount of phase space. However, when using too large time steps, instabilities may arise in the integration. Therefore, the chosen time step should allow for the correct balance between simulating the correct trajectory and covering the phase space. The time steps appropriate for the interaction of some typical motions are shown in Table 1.

Table 1 The different types of motion present in various systems together with suggested time steps.

Systems	Types of motion	Suggested time step (s)
Atoms	Translation	10^{-14}
Rigid molecules	Translation and rotation	5×10^{-15}
Flexible molecules, rigid bonds	Translation, rotation, torsion	2×10^{-15}
Flexible molecules, flexible bonds	Translation, rotation, torsion, vibration	10^{-15} or 5×10^{-16}

In this study, the Verlet algorithm, one of the most widely used methods in molecular dynamics, was chosen for integrating the equations of motion (Verlet, 1967). This algorithm is known to be simple and stable. The advance of positions is approximated from the one-step forward and one-step backward of the Taylor series expansion truncated after the third term:

$$r(r + \delta t) = r(t) + v(t)\delta t + \frac{1}{2}a(t)\delta t^2 + \frac{1}{6}b(t)\delta t^3 \quad (17)$$

$$r(t - \delta t) = r(t) - v(t)\delta t + \frac{1}{2}a(t)\delta t^2 - \frac{1}{6}b(t)\delta t^3 \quad (18)$$

where v is the velocity (the first derivative of the positions with respect to time), a is the acceleration (the second derivative), and b is the third derivative. Summation of the two equations above gives

$$r(t + \delta t) = 2r(t) - r(t - \delta t) + a(t)\delta t^2 \quad (19)$$

Figure 4 shows the flow chart of a molecular dynamics simulation integrated by using the Verlet algorithm. It can be seen that the Verlet algorithm uses the positions and accelerations at time t , and the positions from the previous step, $r(t - \delta t)$, to calculate the new positions at time $t + \delta t$, $r(t + \delta t)$. The velocities do not explicitly appear in this algorithm. However, they can be calculated in a variety of ways. A simple approach is to divide the difference in positions at time $t + \delta t$ and $t - \delta t$ by $2\delta t$:

$$v(t) = \frac{r(t + \delta t) - r(t - \delta t)}{2\delta t} \quad (20)$$

Alternatively, the velocities can be estimated at the half step, $t + 1/2\delta t$:

$$v(t + \frac{1}{2}\delta t) = \frac{r(t + \delta t) - r(t)}{\delta t} \quad (21)$$

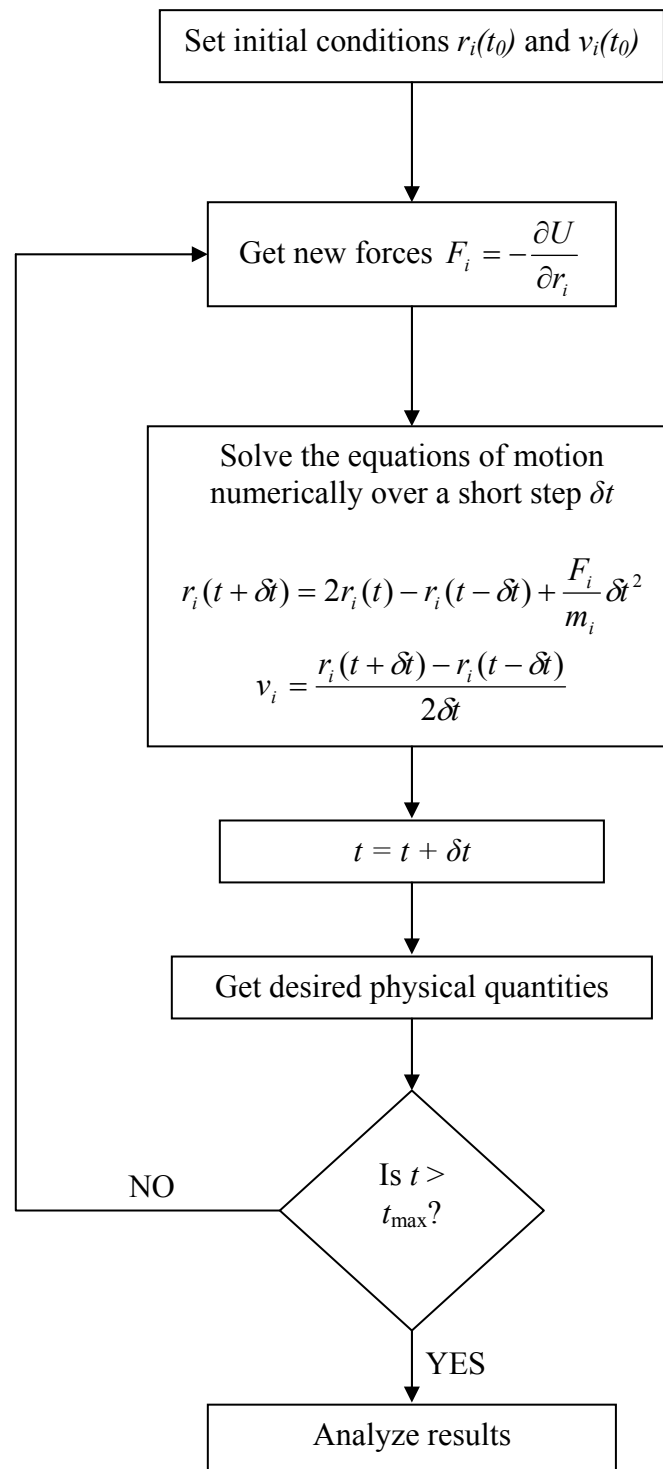


Figure 4 The flow chart of molecular dynamics simulation integrated by using the Verlet algorithm.

Models and methods

1. Ethylene Protonation Reaction on H-FAU

The active sites represented by 3T, 5T, and 7T cluster models shown in Figure 5 (T = Si or Al tetrahedral) are cut out from the crystallographic structure of FAU zeolite (Mortier *et al.*, 1984). At this site, Brønsted proton sitting on bridging oxygen atom O1 of the hexagonal prism linking between two sodalite cages points toward the super cage thus allows large space for the reaction occurs (Hill *et al.*, 1999). In order to generate the cluster model, the dangling bonds of Si and O atoms are capped with H atoms. The distances of dangling bond are 1.47 Å and 0.97 Å for Si-H and O-H, respectively. All calculations were done at the B3LYP level with 6-31G(d,p) basis set using the Gaussian98 program. During the geometry optimizations, only the active region (Si-O-Al-O-Si) atoms were allowed to relax while the other atoms were fixed at the lattice positions. The capped H atoms of the two SiH₃ group and the two OH groups bonded to the Al atom were fixed along the Si-O crystal framework of the zeolite. For the adsorption complex, the transition state and the alkoxide intermediate, both the adsorbate and the active site were optimized. This procedure takes into account the local structure relaxation due to the Al substitution during the Brønsted acid site creation and the interaction of acid site with the adsorbate. The transition state structures were confirmed by the frequency calculations.

Due to the fact that DFT does not account for the dispersion component of the interaction between adsorbate and zeolite, the MP2/6-31G(d,p) single point calculations were carried out at B3LYP/6-31G(d,p) geometries to verify the energetic information between ethylene and the zeolite framework.

To include the effects of the electrostatic potential from zeolite lattice, the optimized structures obtained from bare cluster calculations were embedded in a set of point charges derived by SCREEP method and single point calculation were done at the same level of theory. Note that pure SiO₂ FAU crystal structure was used in calculating the Madelung potential thus Si/Al ratio effects are not included in this

study. Finally, the basis set superposition error has been eliminated by using the full counterpoise correction method (Boys and Bernardi, 1970).

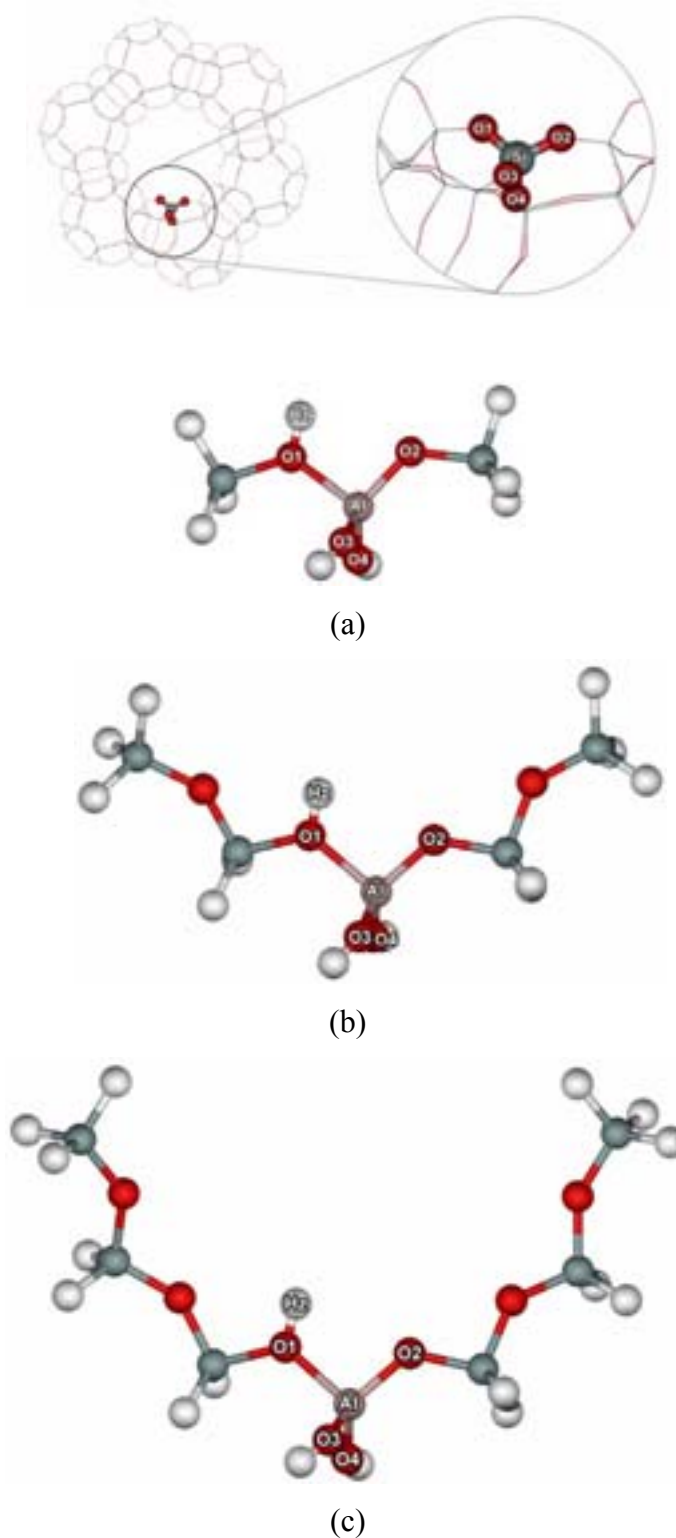


Figure 5 Four different oxygen atoms in the FAU zeolite framework (top) and (a) 3T cluster, (b) 5T cluster, and 7T cluster models with Brønsted proton sitting on oxygen O1.

2. Shape selective adsorption of xylene isomers in H-ZSM-5

The two-layer ONIOM(MP2/6-31G(d,p):UFF) method was used to study the adsorption of *o*-, *m*-, and *p*-xylene in H-ZSM-5 zeolite. A cluster containing 184 tetrahedral (184T) atoms was used to model the H-ZSM-5 zeolite (see Figure 6). The 5T cluster, $\equiv\text{SiOAl}(\text{OSi}\equiv)_2\text{O}(\text{H})\text{Si}\equiv$, with an Al atom replaced at the T12 site was selected as the local active site and noted as the inner layer. This moiety was calculated at MP2/6-31G(d,p) level of theory while the remainder were set as the outer layer and treated with the universal force field (UFF) to represent the confinement by the zeolite framework.

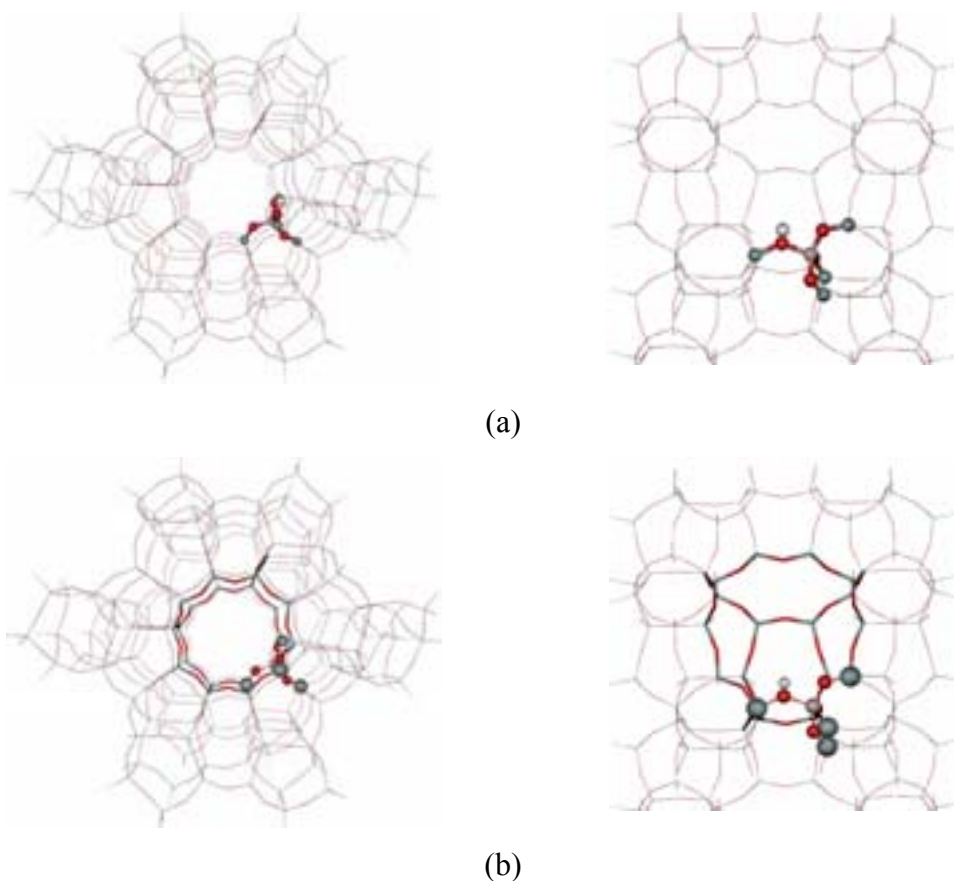


Figure 6 The 184T cluster models viewed along straight channel (left) and zigzag channel (right); (a) the 5T/184T ONIOM(MP2/6-31G(d,p):UFF) and (b) the 5T/23T/184T ONIOM(MP2/6-31G(d,p):B3LYP/6-31G(d,p):UFF).

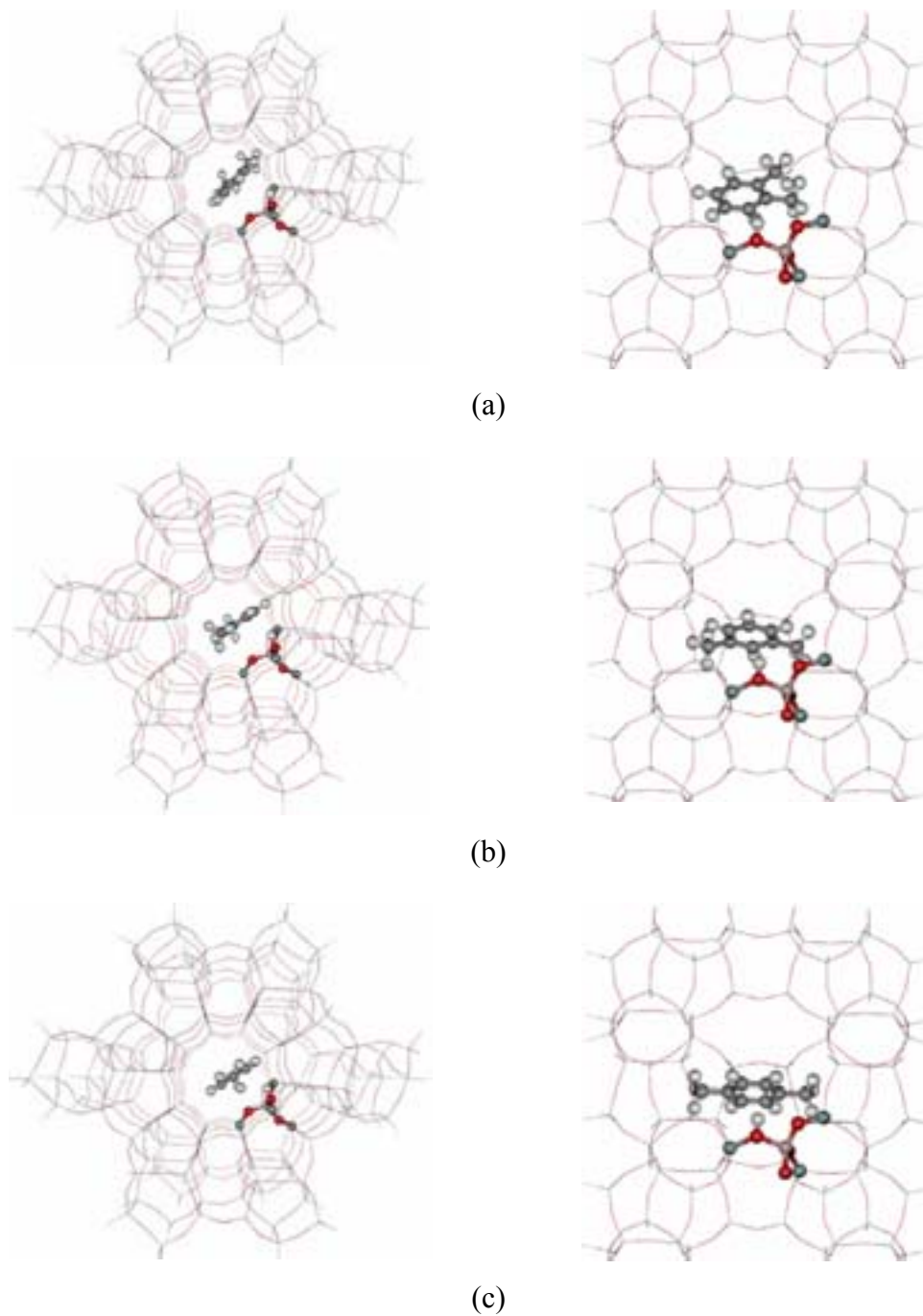


Figure 7 The optimized adsorption structure of (a) *o*-, (b) *m*-, and (c) *p*-xylene in the intersecting channels of H-ZSM-5 viewed the along straight channel (left) and the zigzag channel (right).

To generate the inner layer, the dangling bonds resulting from cutting Si-O bonds at the boundary region were capped with H atoms using the g parameter of 0.8802. Only the constituent atoms of the local active site were allowed to locally relax, whereas the rest was constrained at the crystal positions during the geometry optimization. The capped H-atoms were always aligned along the bond vectors of the real Si-O bonds and the xylene molecules were placed at the intersecting channels without the constraints during the geometry optimization.

Only the most energetically stable configurations of the xylene/zeolite systems obtained by the geometry optimization at ONIOM(HF/3-21G:UFF) method were studied (see Figure 7). To correct the adsorption energies, the three-layered ONIOM(MP2/6-31G(d,p):B3LYP/6-31G(d,p):UFF) scheme was adopted. The quantum mechanical region was extended up to 23T atoms enclosing the adsorption region and the single point energy calculations were carried out using this scheme (see Figure 6). All calculations were performed on Linux workstation using Gaussian03 program.

3. Diffusion mechanism of *p*-xylene in microporous silicalite

3.1. Silicalite structure

Silicalite (the analogous alumino-silicate, ZSM-5) is a pure silica zeolite which has an MFI-type structure. The unit cell is described in the orthorhombic space group Pnma ($a = 20.02$, $b = 19.90$, and $c = 13.38$ Å; $\alpha = \beta = \gamma = 90^\circ$) (Koningsveld, 1990). The framework system is composed of two types of 10-membered-ring pore opening channels: straight channels with an elliptical section, in the flexible zeolite, of about 5.1×5.7 Å, running along the b axis, perpendicularly interconnected by nearly circular zigzag channels ($r \approx 5.4$ Å) running in the direction of the a axis. This particular framework structure provides three possible different sites for adsorbing molecules: at the intersecting channels, within the straight channels, and within the zigzag channels.

3.2. Potential parameters

The interaction model for the flexible zeolite framework used in this work, a generalized valence force field (GVFF), is taken from the work of Nicholas et al. (Nicholas *et al.*, 1991). In this approximation, the potential energy of the framework system is represented by Si-O bond stretches, O-Si-O angle bends, and Si-O-Si angle bends. This particular force field has been confirmed by Smirnov et al. to reproduce experimental vibrational spectra of siliceous zeolites reasonably well (Smirnov and Bougeard, 1993). The Si-O bond stretch and O-Si-O bond bend are approximated as simple harmonic potentials, while the Si-O-Si bond bend, which is highly anharmonic and varies over a wide range in different silicates, is modeled with a quartic potential. The potential energy of the zeolite framework can be written as

$$V_{zeolite} = \frac{k_r}{2}(r - r_0)^2 + \frac{k_\theta}{2}(\theta - \theta_0)^2 + V_{bend}(Si - O - Si) \quad (22)$$

$$V_{bend}(Si - O - Si) = \frac{k'_\theta}{2}(\theta - \theta_0)^2 + \frac{k''_\theta}{3}(\theta - \theta_0)^3 + \frac{k'''_\theta}{4}(\theta - \theta_0)^4 \quad (23)$$

where k_r is the force constant of the Si-O bond stretch, k_θ is the force constant for the O-Si-O angle bend, k'_θ , k''_θ , and k'''_θ are the force constants for the Si-O-Si angle bend, respectively. r and θ are the actual values of bond distances and bond angles, respectively, and the zero indices denote their equilibrium values. The equilibrium bond lengths and bond angles were derived from the structural data of siliceous ZSM-5 (Koningsveld, 1990).

The standard AMBER force field developed by Kollman et al. is employed to evaluate the intramolecular potential for *p*-xylene (Cornell *et al.*, 1995). Four different atom types are defined for the *p*-xylene: CA, CT, HA, HT, and the atoms labeled A belonging to the aromatic ring and those marked T forming part of methyl groups. The functional form of the potential comprises five kinds of terms: harmonic potentials in terms of bond lengths and angles with equilibrium bond lengths and

angles obtained by geometry optimization at the Hartree-Fock (HF) level of approximation using the split-valence 6-31G** basis set. The energies connected with changes in the dihedral angles are represented by a periodic cosine potential function. The (non-bonded) van der Waals interactions are represented by a Lennard-Jones 6-12 potential and Coulomb potentials between sites coinciding with the atomic positions. The values of the point charges were estimated from gas phase population analysis of the corresponding wave functions according to the CHelpG scheme (Breneman and Wiberg, 1990). The point charges of equivalent atoms are equalized to their average values. The non-bonded interactions are only applied for atoms separated by at least three bonds (1-4 interactions) and reduced by using scale factors of 1/1.2 and 1/2 for the 1-4 electrostatic and van der Waals interactions, respectively.

$$V_{xylene} = \frac{k_r}{2}(r - r_0)^2 + \frac{k_\theta}{2}(\theta - \theta_0)^2 + k[1 + \cos(n\phi - \delta)] + \frac{A_{ij}}{r_{ij}^{12}} - \frac{B_{ij}}{r_{ij}^6} + \frac{q_i q_j}{r_{ij}} \quad (24)$$

The intermolecular guest-guest interactions as well as the interactions between guest molecules and the zeolite are expressed, like the non-bonded interactions, as sums of Lennard-Jones (12-6) and Coulomb terms and the parameters for the xylene-xylene interaction are identical in both cases.

$$V_{zeolite-xylene} = \frac{A_{ij}}{r_{ij}^{12}} - \frac{B_{ij}}{r_{ij}^6} + \frac{q_i q_j}{r_{ij}} \quad (25)$$

where i refers to the sites on silicalite and j on p -xylene. A_{ij} and B_{ij} are energy parameters characteristic of the i - j interaction, q_i is the partial charge associated with the site. r_{ij} is the distance between two sites.

The short-range Lennard-Jones interactions of zeolite-xylene are taken from the works of Catlow *et al.* (1991). Only the interactions between xylene atoms and the O-atoms of the zeolite framework are taken into account, while interactions with Si atoms are ignored since they are well shielded by the oxygen atoms of the SiO₄

tetrahedra. Mulliken charges, evaluated from periodic Hartree-Fock calculations of siliceous sodalite using split-valence 6-21G* basis set, were determined for Si and O atoms of the zeolite framework. All detailed of the interaction model and the full set of parameters are documented in Tables 2-5.

Table 2 The potential parameters of silicalite zeolite.

Parameters	Equilibrium values	Force constants
Si-O	$r_0 = 1.591^a$	$k_r = 597.32^b$
O-Si-O	$\theta_0 = 109.5^c$	$k_\theta = 138.12^d$
Si-O-Si	$\theta_0 = 155.0^c$	$k'_\theta = 10.85^d$ $k''_\theta = -34.08^e$ $k'''_\theta = 26.52^f$
Atomic charges	Si	O
e	2.000	-1.000

^aÅ. ^bkcal/(mol·Å²). ^cDegrees. ^dkcal/(mol·rad²). ^ekcal/(mol·rad³). ^fkcal/(mol·rad⁴).

Table 3 The potential parameters of xylene isomers.

Bond	k_r (kcal/mol·Å ²)	r_0 (Å)	
CA-CA	938.00	1.387	
CA-HA	734.00	1.076	
CA-CT	634.00	1.510	
CT-HT	680.00	1.085	
Angle	k_r (kcal/mol·Å ²)	θ_0 (Degrees)	
CA-CA-CA	126.00	120.00	
CA-CA-HA	70.00	120.00	
CA-CA-CT	140.00	120.00	
CA-CT-HT	100.00	109.50	
HT-CT-HT	70.00	109.50	
Dihedral	k (kcal/mol)	n	δ (Degrees)
X-CA-CA-X	3.6250	2.0	180.0
X-CA-CT-X	0.0000	2.0	0.0

Table 4 Partial charges of different atoms in *p*-xylene.

Atomic Charges	$ e $
CA1 ^a	-0.205
CA2 ^b	0.180
CT	-0.222
HA	0.130
CT	0.064

^aAromatic C atom attached by CH₃^bAromatic C atom attached by H

Table 5 The potential parameters of xylene-xylene and zeolite-xylene interaction.

Lennard-Jones	A_{ij} (kcal.Å ¹² /mol)	B_{ij} (kcal.Å ⁶ /mol)
CA-CA	819971.6622	531.10286
CA-HA	76245.1550	104.66068
HA-HA	5716.2960	18.51966
CT-CT	1043080.2307	675.61225
CT-HT	97170.8117	126.91915
HT-HT	7516.0770	21.72578
CA-CT	924822.2697	599.01553
CA-HT	86154.1883	112.52984
HA-CT	85994.7003	118.04375
HA-HT	6558.2560	20.06420
CA-O	346035.0000	516.79174
HA-O	35904.5916	128.53355
CT-O	253759.0000	407.26013
HT-O	35904.5916	128.53355

3.3. Molecular dynamics simulations

The simulated system consists of $2 \times 2 \times 4$ unit cells of silicalite with a total of 4608 atoms (1536 Si atoms and 3072 O atoms). The initial atomic coordinates were taken from the powder X-ray diffraction data of ZSM-5 with a Si/Al ratio of 299. Orthorhombic periodic boundary conditions are applied to include the effects of the infinite framework. Xylene loadings of 16, 32, 48, and 64 molecules in a silicalite supercell, corresponding to 1, 2, 3, and 4 molecules/unit cell, are studied. The guest molecules are initially randomly placed at the intersecting channels. These different loadings are modeled with the same periodic boundary conditions. The electrostatic interactions are computed by using the Ewald sum method, and the van der Waals interactions are evaluated within a cutoff radius of 12 Å. All MD simulations are carried with the program DLPOLY, version 2.0.

The simulations are performed within the microcanonical ensemble (NVE) at average temperatures of 300, 400, and 500 K. The initial velocities of all atoms are assigned according to a Maxwell-Boltzmann distribution corresponding to the reference temperatures. The Verlet algorithm is used with an integration time step of 1 fs. After 50 ps equilibration period, the velocity rescaling algorithm is removed and a run of 20 ps is performed to ensure that there are no further drifts. After that the coordinates and velocities of the atoms are stored every 80 fs for an additional 1 ns run for later analysis. In selected cases, production runs have been extended up to 2 ns.

4. Adsorption and diffusion of *p*-xylene in mesoporous Si-MCM-41

4.1. Construction of the Si-MCM-41 structure

From high resolution electron microscopy measurements, it was concluded that the pores of MCM-41 have essentially one-dimensional cylinder-like shapes and are arranged parallel to each other in a honeycomb-type lattice, without intersections. These materials can be prepared with pore diameters ranging from 15 to 100 Å (Beck *et al.*, 1992). Interestingly, both circular and hexagonal cross sections have been visualized (Chenite *et al.*, 1995). Although the structure of MCM-41 has been extensively studied, detailed crystallographic data at the atomic level are still lacking. In this study, the high-silica form of amorphous MCM-41 was modelled as a hypothetical Si-MCM-41 perfect lattice. The simulations were performed on an orthorhombic supercell ($a = 39.37 \text{ \AA}$, $b = 22.73 \text{ \AA}$, $c = 45.99 \text{ \AA}$; $\alpha = \beta = \gamma = 90^\circ$) comprising 1440 atoms (480 Si atoms and 960 O atoms). Each supercell contained two parallel hexagonal channels running along the c-axis, as illustrated in Figure 8.

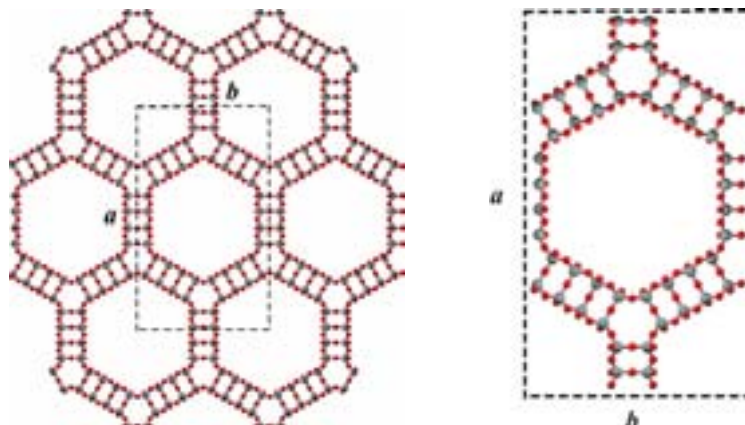


Figure 8 Model of Si-MCM-41; the hexagonal lattice framework (left) and the Si-MCM-41 supercell (right).

4.2. Potential parameters

It is known that when guest molecules diffuse inside the pores of certain zeolites, the conformation of the zeolite is modified to a certain extent in order to achieve the best energetic and shape complementarity with the guest molecules. In some cases, diffusion is not possible at all without a concomitant deformation of the lattice. Furthermore, especially at lower loadings, the thermalization of guest molecules can be achieved only through the lattice framework (Schrimpf *et al.*, 1992). Thus, both the MCM-41 framework and *p*-xylene were modelled as flexible entities in order to mimic these features of the real systems as closely as possible.

The interaction model for the lattice and *p*-xylene are identical to the ones used in silicalite system. The equilibrium bond lengths and bond angles were derived from structural data. In modelling the framework flexibility of our hypothetical Si-MCM-41, we were guided by the experimental vibrational spectra. It has been shown that the inclusion of additional non-bonded long range or cross terms does little to improve the structure and the quality of the vibrational spectra (Ermoshin *et al.*, 1996). By taking advantage of this, such terms were not included in the calculations.

The intermolecular guest-guest interactions as well as the interactions between guest molecules and MCM-41 were expressed, like the non-bonded interactions, as sums of Lennard-Jones (LJ 12-6) and Coulomb terms between atomic sites. The LJ- and charge parameters for xylene are identical in both cases.

$$V_{MCM-xylene} = \sum \left[4\varepsilon_{ij} \left[\left(\frac{\sigma_{ij}}{r_{ij}} \right)^{12} - \left(\frac{\sigma_{ij}}{r_{ij}} \right)^6 \right] + c \cdot \frac{q_i q_j}{r_{ij}} \right] \quad (26)$$

where i refers to the sites on Si-MCM-41 and j on p -xylene. ε_{ij} and σ_{ij} are energy and size parameters characteristic of the i - j interaction, q_i is the partial charge associated with the site and c is a constant. r_{ij} is the distance between two sites.

The LJ-parameters between p -xylene and the atomic framework of MCM-41 were derived by fitting to the experimental heat of adsorption of p -xylene in Si-MCM-41. Half the formal charges were assigned to the Si and O atoms of the Si-MCM-41 framework (Nicholas and Hess, 1994). The resulting potential parameters are listed in Table 6.

Table 6 Potential parameters for short-range interactions between *p*-xylene and Si-MCM-41.

Lennard-Jones parameters	ϵ (kcal/mol)	σ (Å)
CA-Si	0.0643	3.57
HA-Si	0.0269	3.17
CT-Si	0.0724	3.57
HT-Si	0.0275	3.20
CA-O	0.1173	3.17
HA-O	0.0490	2.77
CT-O	0.1321	3.17
HT-O	0.0501	2.80

4.3. Molecular dynamics simulations

The simulations were performed in the NVE-ensemble at room temperature (300 K) with the DLPOLY program on a modern Linux workstation. Orthorhombic periodic boundary conditions were applied to include the effects of the infinite framework. Additionally to runs with only one xylene guest molecule, loadings of 16, 32, 48, and 64 molecules per Si-MCM-41 supercell, corresponding to 8, 16, 24, and 32 molecules per hexagonal channel in our box, or experimental loadings of roughly 0.55, 1.11, 1.66, and 2.22 mmol of *p*-xylene per gram of Si-MCM-41 (mmol/g), were simulated. The different loadings were modelled with the same periodic boundary condition. The electrostatic interactions were computed using the Ewald sum method and the van der Waals interactions were evaluated within a cutoff-radius of 11 Å. The Verlet algorithm was used with an integration time step of 1 fs.

The starting configurations of the mesopore-xylene systems were first equilibrated by running a simulation at 0 K for 50 ps using a strongly coupled thermostat. This is a crude energy minimizer to help the system to relax before a

simulation begins. The last configuration from this run was used as input for a 100 ps equilibration period at the desired temperature, 300 K (velocity rescaling). After this period, the velocity rescaling algorithm was removed and a run of 50 ps was performed to ensure that there were no further drifts. After that the coordinates and velocities of the atoms were stored every 10 fs for an additional 100 ps run for later analysis.

RESULTS AND DISCUSSION

Chapter I: Ethylene protonation reaction on H-FAU zeolite

1. Brønsted active site

The selected parameters of 3T, 5T and 7T cluster models for H-FAU zeolite are listed in Table 7. It can be seen that a number of oxygen atoms added in the larger cluster size have an effect on the lengthening of O1-Hz bond distance (see Figure 9). This results in the more positive charge on Hz and thus eases the protonation of Brønsted proton. On the other hand, it suggests that the interaction between the Brønsted site and basic adsorbates is stronger in the larger cluster. The active sites predicted by the 5T and 7T cluster models are almost equivalent while those obtained from the 3T are quite different. With respect to the bare cluster model, the charge value on Brønsted proton estimated by embedded cluster single point calculation is more positive. This reflects that the electrostatic potential from the extended lattice has a significant effect on enhancing the acidity of the zeolite which is the same conclusion as previous studies (Limtrakul *et al.*, 2001). One anticipates that the ionic-like nature of the transition state might be effectively stabilized by the Madelung potential from the zeolite framework.

Table 7 Selected B3LYP/6-31G(d,p) parameters of active site of H-FAU zeolite calculated by using 3T, 5T and 7T cluster models (see Figure 9). Bond lengths are in Å and bond angles in degrees. The values in the bracket are estimated by embedded cluster single point calculation.

Geometry	3T cluster	5T cluster	7T cluster
<i>Distances</i>			
O1-Hz	0.967	0.969	0.969
Al-O1	1.919	1.915	1.915
Al-O2	1.711	1.705	1.705
Si1-O1	1.712	1.702	1.700
Si2-O2	1.638	1.618	1.617
<i>Angles</i>			
∠O1-Al-O2	96.8	98.1	98.0
∠Si1-O1-Al	127.0	126.7	126.6
∠Si2-O2-Al	127.2	128.2	128.2
<i>Charges (e)</i>			
q_{Hz}	+0.568 [+0.575]	+0.572 [+0.581]	+0.574 [+0.587]

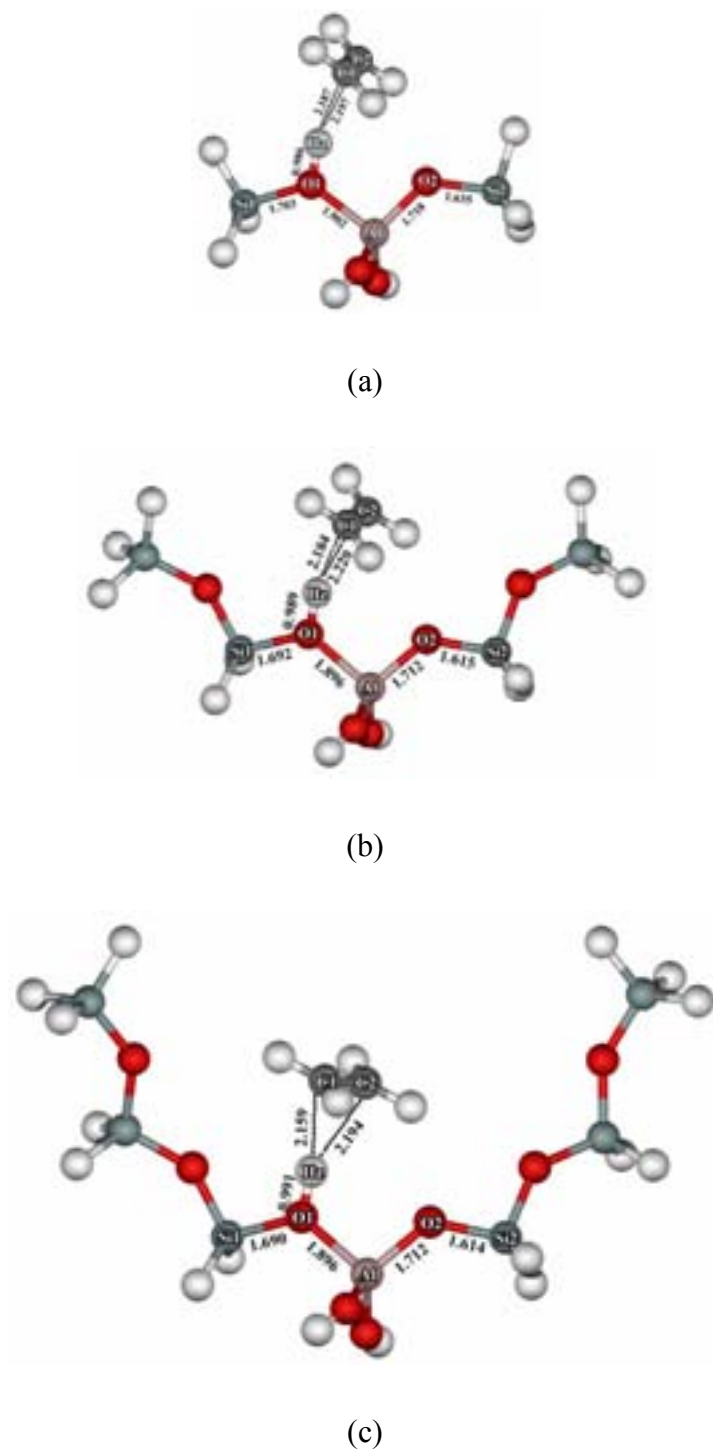


Figure 9 The optimized adsorption structures of ethylene on H-FAU using (a) 3T, (b) 5T, and (c) 7T cluster models.

2. Adsorption complex

The selected geometry parameters of ethylene adsorption on H-FAU have been shown in Table 8 and displayed in Figure 9. It has been found that the geometry of the π -complex is similar to the geometry of isolated reactants. For instance, the O1-Hz bond distance, on average, increases only 0.02 Å from the isolated zeolite cluster to the π -complex, and the C1-C2 bond distance, on average, increases only 0.01 Å from isolated ethylene to the π -complex. The C1-C2 bond distance of ethylene in the π -complex is not affected by the size of zeolite model. However, as the cluster size increases, the changes in C1-Hz, C2-Hz and O1-Hz bond distances can be observed. The C1-Hz and C2-Hz distances are almost equivalent in the 3T cluster, but the larger differences have been found in the 5T and 7T clusters (see Figure 9). The O1-Hz bond distance is substantially elongated, going from 0.986 Å in 3T cluster to 0.991 Å in 7T cluster according to the stronger interaction of the ethylene molecule to the Brønsted proton.

The adsorption energies of ethylene on zeolite model have been calculated as the differences in the total energy between the ethylene π -complex and isolated reactants. The corrected adsorption energies including the basis set superposition error estimated by the full counterpoise correction method have been calculated at both B3LYP and MP2 levels (see Table 8). The relative stability of the π -complex slightly increases when the cluster size employed is larger. The B3LYP adsorption energies have been estimated to be -5.46 to -5.77 kcal/mol from 3T cluster to 7T cluster. Adding the dispersion interaction calculated at the MP2 level enhances the adsorption energies to be -5.79 to -6.69 kcal/mol from 3T cluster to 7T cluster. The inclusion of the Madelung potential from the extended lattice increases the adsorption energy only 1-2 kcal/mol at both B3LYP and MP2 levels. The MP2 embedded adsorption energy of -8.62 kcal/mol agrees well with the experimental observation reported by Cant and Hall of -9 kcal/mol (Cant and Hall, 1972).

Table 8 Selected B3LYP/6-31G(d,p) structural parameters and corrected adsorption energies (kcal/mol) of [C₂H₄]/H-FAU complexes calculated by using 3T, 5T and 7T cluster models. Bond lengths are in Å and bond angles in degrees. The values in the bracket are estimated by embedded cluster single point calculation.

Geometry	3T cluster	5T cluster	7T cluster
<i>Distances</i>			
C1-C2 ^a	1.337	1.337	1.338
C1-Hz	2.187	2.184	2.159
C2-Hz	2.197	2.220	2.194
O1-Hz	0.986	0.989	0.991
Al-O1	1.902	1.896	1.896
Al-O2	1.718	1.712	1.712
Si1-O1	1.703	1.692	1.690
Si2-O2	1.635	1.615	1.614
<i>Angles</i>			
∠O1-Al-O2	97.7	98.9	98.9
∠Si1-O1-Al	126.6	126.2	126.0
∠Si2-O2-Al	128.5	129.5	129.5
<i>Charges (e)</i>			
q _{O1}	-1.136	-1.155	-1.156
q _{O2}	-1.282	-1.288	-1.287
<i>Adsorption Energies</i>			
B3LYP+BSSE ^b	-5.46 [-6.47]	-5.38 [-6.97]	-5.77 [-7.86]
MP2+BSSE ^c	-5.79 [-6.73]	-6.28 [-7.76]	-6.69 [-8.62]

^aThe calculated B3LYP/6-31G(d,p) of C=C bond distance in gas phase is 1.330 Å.

^bThe BSSE-corrected adsorption energy calculated at B3LYP/6-31G(d,p). ^cThe BSSE-corrected adsorption energy calculated at MP2/6-31G(d,p) using the B3LYP/6-31G(d,p) optimized structure.

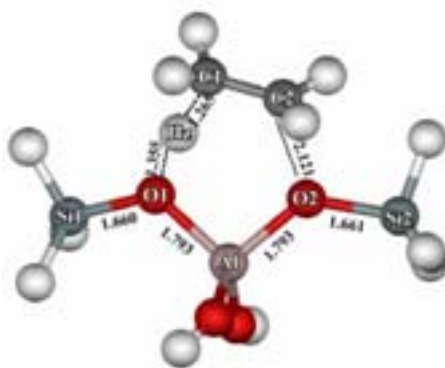
3. Transition state

Table 9 and Figure 10 show all selected geometry parameters of transition state. At this stage, the proton of zeolite is migrating toward C1 atom of ethylene. Simultaneously, C2 moves toward O2 of zeolite lattice. The C1-C2 bond distance is thus longer with respect to the π -complex. As illustrated in Figure 10, the acidic proton is halfway between C1 of ethylene molecule and O1 of zeolitic active site. In all models, the proton is closer to the carbon atom than the active site oxygen atom. It can be seen that, as the cluster size increases, the zeolitic proton comes closer to contact with C1 of ethylene and makes the O1-Hz longer. This indicates that the protonation process is facilitated upon increasing the cluster size. However, the effect of cluster size does not change the C1-C2 bond distance (1.404 Å) which is in between the single bond and double bond. A longer distance between C2 and O2 is also observed with increasing the cluster size. Using a more realistic model of the 7T cluster provides a more ionic-like structure of the transition states. According to the population analysis, the positive charge on $C_2H_5^+$ fragments of the transition state increases from +0.584e at 3T cluster to +0.671e at 7T cluster. The effects of Madelung potential tend to increase the ionicity of the system. The positive charges on $C_2H_5^+$ fragment increase by about 0.02-0.04e with respect to the bare cluster calculation. This result follows the same trend as obtained in the transition state of ethylene protonation on theta-1 zeolite reported by Corma and coworkers (*Boronat et al.*, 2001a). It is found that, in the transition state structures, the zeolite active sites allowed to relax during the optimization provide slightly different bond lengths in both sides of Al atom (Al-O1, Al-O2, Si1-O1, and Si2-O2).

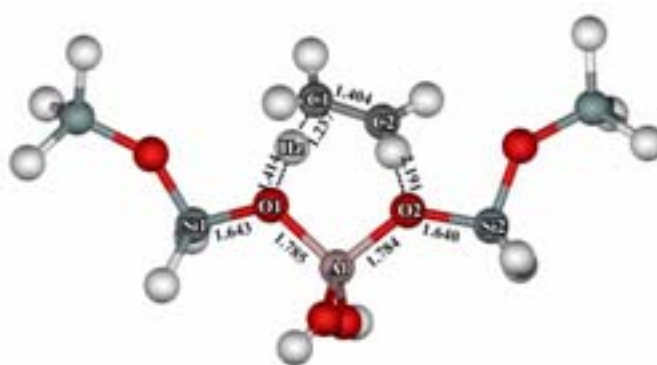
Table 9 Selected B3LYP/6-31G(d,p) structural parameters and corrected activation energies (kcal/mol) of [C₂H₄]/H-FAU transition states calculated by using 3T, 5T and 7T cluster models. Bond lengths are in Å and bond angles in degrees. The values in the bracket are estimated by embedded cluster single point calculation.

Geometry	3T cluster	5T cluster	7T cluster
<i>Distances</i>			
C1-C2	1.404	1.404	1.404
C1-Hz	1.265	1.237	1.230
O1-Hz	1.355	1.414	1.428
O2-C2	2.121	2.191	2.204
Al-O1	1.793	1.785	1.785
Al-O2	1.793	1.784	1.784
Si1-O1	1.660	1.643	1.641
Si1-O2	1.661	1.640	1.638
<i>Angles</i>			
∠O1-Al-O2	98.5	99.8	99.7
∠Si1-O1-Al	124.0	124.0	124.0
∠Si2-O2-Al	130.1	130.9	130.7
<i>Charge (e)</i>			
<i>q</i> _{O1}	-1.217	-1.236	-1.238
<i>q</i> _{O2}	-1.170	-1.197	-1.200
<i>q</i> _{C2H5+}	+0.584 [+0.601]	+0.623 [+0.647]	+0.633 [+0.671]
<i>Activation energies</i>			
B3LYP+BSSE ^a	18.32 [14.48]	17.77 [10.80]	17.11 [8.68]
MP2+BSSE ^b	24.38 [20.26]	23.05 [15.63]	22.33 [13.23]

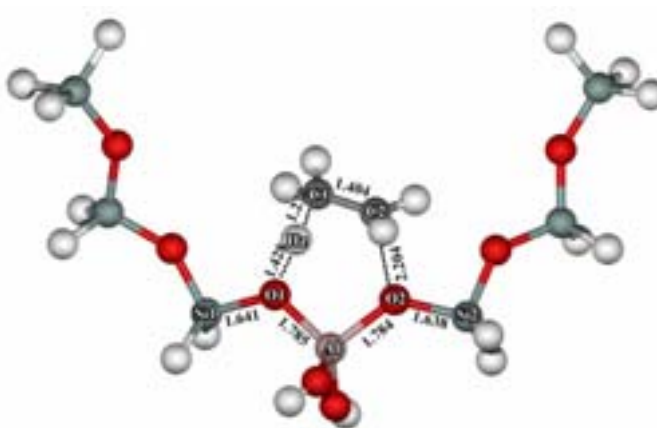
^aThe BSSE-corrected adsorption energy calculated at B3LYP/6-31G(d,p). ^bThe BSSE-corrected adsorption energy calculated at MP2/6-31G(d,p) using the B3LYP/6-31G(d,p) optimized structure.



(a)



(b)



(c)

Figure 10 The optimized structures of ethylene protonation transition state using (a) 3T, (b) 5T, (c) 7T cluster models.

The activation energies evaluated in Table 9 were calculated as the total energy difference between the transition state and isolated reactants. The same trend has been observed at both B3LYP and MP2 levels. The activation energies with the BSSE correction slightly decrease from 3T cluster to 7T cluster (only 1 kcal/mol at B3LYP level and 2 kcal/mol at MP2 level). When the dispersion component is included by means of MP2, the activation energies is increased between 5 and 6 kcal/mol with respect to the B3LYP calculations (see also Table 9). With the inclusion of the Madelung potential from the zeolite lattice, the activation energy was found to strongly depend on the cluster size models. The stabilization of the transition state affected by the increase of the cluster size varies between 4 and 9 kcal/mol at both B3LYP and MP2 levels. Similar to bare cluster calculation, the MP2 activation energies are greater than that of B3LYP by 5-6 kcal/mol.

4. Surface ethoxide formation

The final step of reaction is the covalent bond formation of surface ethoxide. In this step, C2 of ethylene has already bonded to O2 of zeolite lattice with the C-O covalent bond as shown in Figure 11. It can be seen that the surface alkoxide formed in 3T cluster is highly stable with the shorter distance in C-O bond compared to the larger clusters. In contrast to the 3T cluster, the oxygen sites in larger clusters play an important role in constraining the orientation of ethyl group. This effect yields the longer distance of C-O bond found in 5T and 7T clusters. The C-C double bond of ethylene molecule is completely changed to single bond at this stage. All geometry parameters of surface alkoxide are shown in Table 10.

The reaction energies have been calculated as the total energy difference between the surface ethoxide and isolated reactants (see Table 10). It is found that the surface ethoxide formation is exothermic reaction. As mentioned above, the reaction energy of a very stable covalent bond formation of surface ethoxide in 3T cluster is higher than that of 5T and 7T clusters. In contrast with the bare cluster calculation, the surface ethoxide formed in 3T cluster is less stable in relation to 5T and 7T clusters when the effects of zeolite framework have been taken into account. However, the

effects of Madelung potential from zeolite frame work have been found to enhance the stability of surface ethoxide by about 3 kcal/mol in 3T cluster and 7 kcal/mol in 5T and 7T clusters. The increasing stability of the surface ethoxide of about 3 kcal/mol has been obtained when the dispersion interaction is included by means of MP2 calculation.

Table 10 Selected B3LYP/6-31G(d,p) structural parameters corrected reaction energies (kcal/mol) of [C₂H₄]/H-FAU surface ethoxides calculated by using 3T, 5T and 7T cluster models. Bond lengths are in Å and bond angles in degrees. The values in the bracket are estimated by embedded cluster single point calculation.

Geometry	3T cluster	5T cluster	7T cluster
<i>Distances</i>			
C1-C2	1.516	1.515	1.515
O2-C2	1.497	1.512	1.513
Al-O1	1.723	1.718	1.719
Al-O2	1.926	1.909	1.909
Si1-O1	1.635	1.619	1.618
Si1-O2	1.718	1.703	1.702
<i>Angles</i>			
∠O1-Al-O2	97.4	98.7	98.6
∠Si1-O1-Al	119.9	120.5	120.5
∠Si1-O2-Al	131.4	131.3	131.3
<i>Charges (e)</i>			
<i>q</i> _{O1}	-1.282	-1.288	-1.288
<i>q</i> _{O2}	-0.960	-0.982	-0.984
<i>Reaction energies</i>			
B3LYP+BSSE ^a	-14.38 [-17.47]	-12.52 [-19.79]	-12.71 [-19.34]
MP2+BSSE ^b	-17.10 [-20.35]	-15.71 [-23.02]	-15.58 [-22.57]

^aThe BSSE-corrected adsorption energy calculated at B3LYP/6-31G(d,p). ^bThe BSSE-corrected adsorption energy calculated at MP2/6-31G(d,p) using the B3LYP/6-31G(d,p) optimized structure.

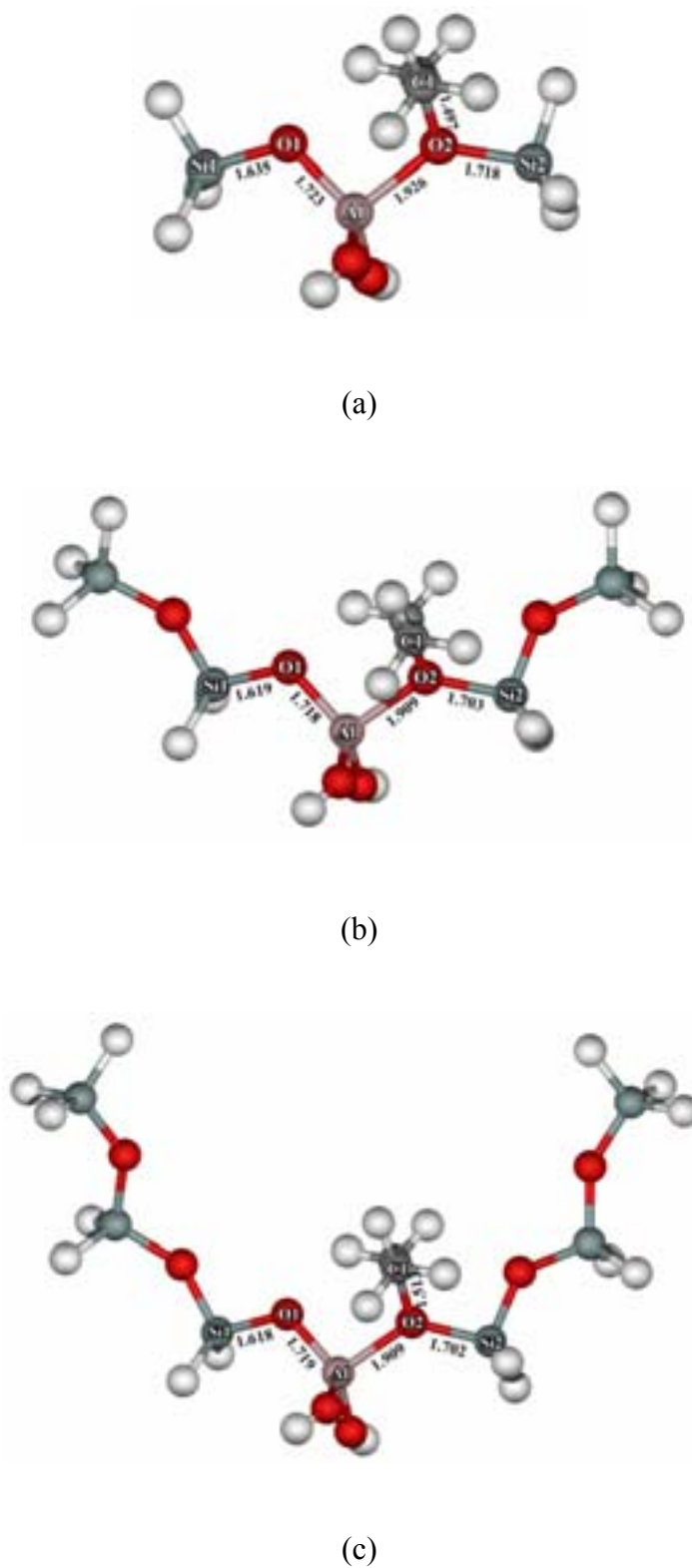


Figure 11 The optimized structures of surface ethoxide using (a) 3T, (b) 5T, (c) 7T cluster models.

5. Mechanistic aspects of the ethylene protonation on H-FAU

The mechanism of ethylene protonation reaction can be summarized as follows. The first step is the migration of ethylene to the Brønsted active site and adsorbs on OH group of zeolite as a π -complex, where the hydrogen atom of OH group is directed toward the double bond C1-C2 of ethylene. Subsequently, the acidic proton transfers from the zeolitic framework to protonate ethylene molecule resulting in the formation of C-O covalent bond of alkoxide product. The protonation reaction was confirmed to occur via by the reaction coordinate frequency at the transition state. At this stage, the covalent bond formation simultaneously occurs with the protonation process. It was found that the surface ethoxide formation in H-FAU is exothermic which differs from endothermic reaction in theta-1 zeolite reported by Corma and coworkers (Boronat *et al.*, 2001a). When the protonation process occurs, the negative charge on O1 of zeolite is increased whereas the negative charge on O2 is decreased. These behaviors result in the strong repulsion of nonbonding electron cloud on O1 atom and makes Si1-O1-Al bond angle decreases through the reaction progress. In the opposite way, the reduction of nonbonding electron cloud on O2 atom due to the covalent bond formation results in the increasing Si2-O2-Al bond angle.

From the geometry changes, it can be seen that 3T cluster model is not large enough to represent the local structure of zeolite active site in this system because the boundary hydrogens are in the position that can directly interact with the adsorbate. As shown in Figures 9, the orientation of ethylene molecule is almost perpendicular to the zeolite cluster backbone. This is due to the repulsive interaction between boundary hydrogen of zeolite model and hydrogen atoms of ethylene molecule. Instead, the bridging oxygen atoms added adjacent to the active site in the larger cluster models can weakly form hydrogen bond with ethylene molecule (see also Figure 10). In contrast with the bare cluster calculation, the embedded cluster single point calculation of surface ethoxide formed in 3T cluster is less stable than that of 5T and 7T clusters. This confirms that the alkoxide complex formed in 3T cluster does not exactly correspond to the optimized geometry in the interior of the zeolite cavity.

Furthermore, the zeolitic backbone geometry of 3T cluster is also quite different from other larger clusters.

The BSSE correction does not change the trend of the results. The same trends are obtained in both bare and embedded cluster approaches. As the cluster model size increases, the adsorption complex and the transition state are more stabilized whereas the surface ethoxide is more slightly destabilized. With the inclusion of the Madelung potential from the zeolite lattice, the adsorption complex, transition state and surface alkoxide are more stable than that of bare cluster calculation. The larger cluster size employed yields the adsorption energy closer to the experimental observed. The destabilization of surface ethoxide observed in the larger cluster size can be explained by the weakening covalent bond nature from the C-O bond lengthening. It is to note that the transition state activation energy is strongly dependent on the cluster size. This is due to the known fact that the loosely bound electrons of transition state are more delocalized than that of adsorption complex and surface alkoxide (Vos *et al.*, 2002), therefore the larger cluster used provides a larger space for electron delocalization and leads to the more stable transition state. Because of the ionic nature of the transition state, therefore, the electrostatic potential is essentially needed.

When the dispersion component is taken into account (see Table 8), the adsorption complex and surface alkoxide are more stable which is in contrast with the transition state that are less stable in relation to B3LYP level. The activation energies obtained from embedded 7T cluster of 8.7 kcal/mol at B3LYP level seems to be underestimated when compared to 13.2 kcal/mol at MP2 level. The later activation energy value is comparable with the experimental estimation of 16 kcal/mol reported by Cant and Hall (1972).

Chapter II: Shape-selective adsorption of xylene isomers in H-ZSM-5

1. Adsorption structures

The adsorption complexes of *o*-, *m*-, and *p*-xylene in the intersecting channels of H-ZSM-5 are shown in Figure 7 (29). It can be seen that the three xylene isomers interact with the active site via a hindered and distorted H-bond. The proton of the active site is pushed aside from the bare active site to interact with the π -bond of the xylene molecules in the intersecting channels. The interaction between acidic proton and the π -bond results in weakening the O1-Hz bond, thus increasing the O1-Hz bond distance by 0.004, 0.010, and 0.011 Å for *o*-, *m*-, and *p*-xylene, respectively (see Table 11 and Figure 12). For the *o*-xylene isomer, this interaction is very weak as compared with other isomers. The C1-C2 bond, which is the π -bond closest to the acidic proton, is not different from the isolated *o*-xylene. This is due to the steric hindrance of the two methyl groups that are prevented by the zeolite framework to approach the acidic site (C1-Hz = 2.982 and C2-Hz = 3.170 Å). In the case of *m*- and *p*-xylene, the most stable adsorption configurations allow them to interact more strongly with the active site, as determined by the shorter distances of C1-Hz and C2-Hz distances (2.448 and 2.597 Å for *p*-xylene and 2.538 and 2.581 Å for *m*-xylene, respectively). The C1-C2 bond distances increase by 0.002 and 0.006 Å for *m*- and *p*-xylene, respectively. The bond stretching and bond contracting of the zeolite active site upon the adsorption process follow Guttmann's rule, i.e. the elongation of O1-Hz bond results in the Al-O1 bond contracting and the lengthening of the Si-O1 bond. The changes in bond angles are observed within about 1-2° (see Table 11).

Table 11 Selected geometrical parameters and adsorption energies of *o*-, *m*-, and *p*-xylene adsorbed in H-ZSM-5 (see also Figure 12). The values in parentheses belong to the isolated xylene.

Parameter	H-ZSM-5	<i>o</i> -C ₈ H ₁₀	<i>m</i> -C ₈ H ₁₀	<i>p</i> -C ₈ H ₁₀
<i>Distances</i> (Å)				
C1-C2	-	1.399 (1.399)	1.397 (1.395)	1.402 (1.396)
C1-Hz	-	2.982	2.538	2.448
C2-Hz	-	3.170	2.581	2.597
O1-Hz	0.968	0.972	0.978	0.979
Al-O1	1.793	1.787	1.784	1.785
Al-O2	1.660	1.662	1.657	1.657
Si1-O1	1.676	1.681	1.679	1.678
Si2-O2	1.598	1.596	1.590	1.590
<i>Angles</i> (°)				
∠O1-Al-O2	90.0	90.8	91.2	91.2
∠Si1-O1-Al	132.5	131.7	131.2	131.4
∠Si2-O2-Al	131.3	131.9	133.0	132.8
Adsorption energies (kcal/mol)				
E _{ONIOM2} ^a		-38.00	-39.24	-38.96
E _{ONIOM3} ^b		-18.03	-21.16	-21.75

^aThe adsorption energies calculated at ONIOM(MP2/6-31G(d,p):UFF). ^bThe adsorption energies calculated at ONIOM(MP2/6-31G(d,p):B3LYP/6-31G(d,p):UFF)

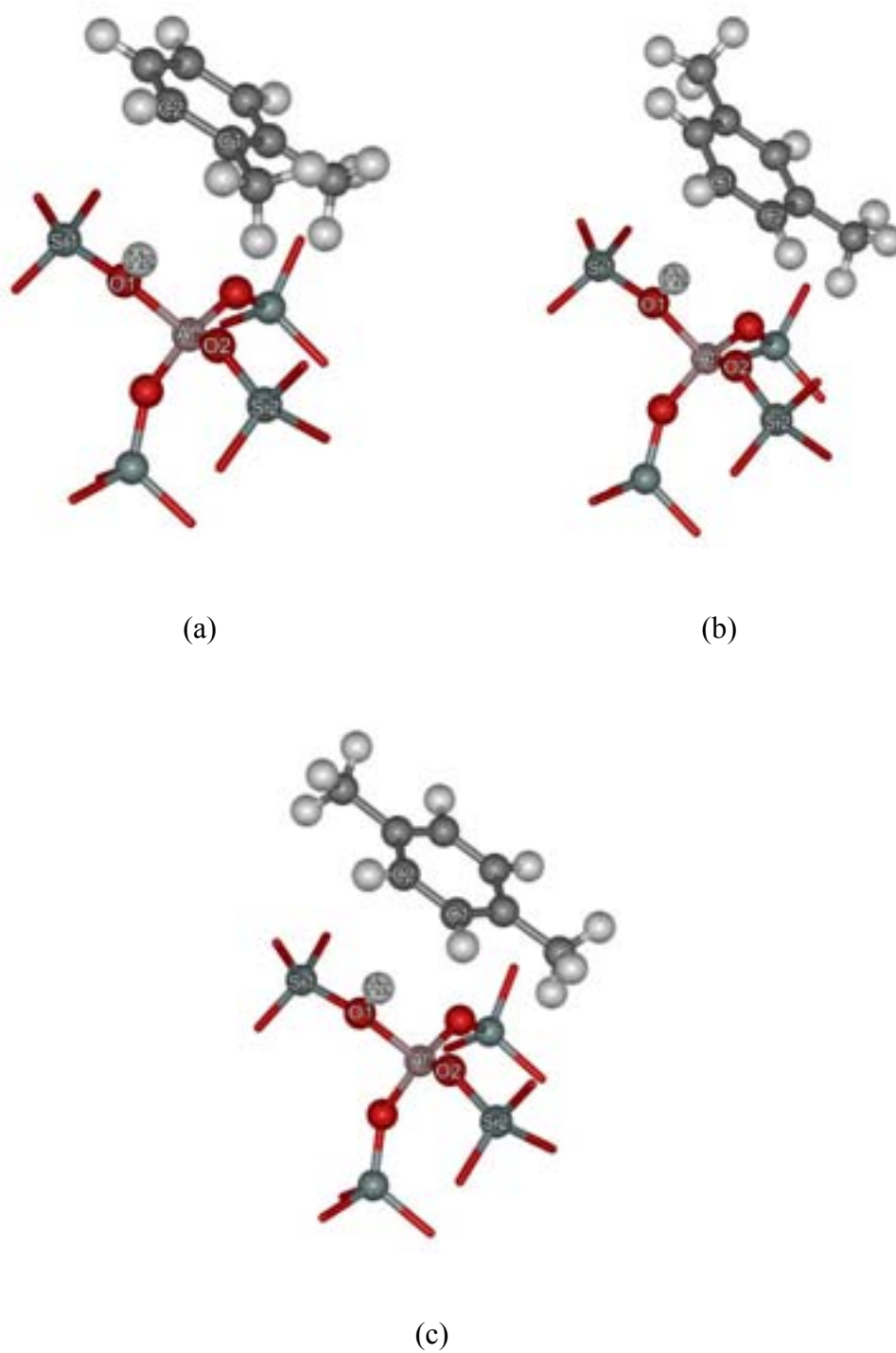


Figure 12 The adsorption complex of (a) *o*-xylene, (b) *m*-xylene, and (c) *p*-xylene in the intersecting channel of H-ZSM-5. The extended framework is omitted for clarity.

2. Adsorption energies

The adsorption energies of three xylene isomers are listed in Table 11. In order to find realistic configurations of the xylene isomers in zeolite pores, the full effect of the confinement by the zeolite framework has to be included. The UFF force field has been proven to provide reasonable geometries with only a little increase in computational demand (Kasuriya *et al.*, 2003; Panjan *et al.*, 2003). However, this force field was found to give overestimated adsorption energies, especially in systems where the molecular size of adsorbed molecule is tightly fitted in the zeolite pores (Raksakoon *et al.*, 2003; Rungsirisakun *et al.*, 2004). As seen in Table 11, the ONIOM(MP2/6-31G(d,p):UFF) adsorption energy of *o*-, *m*-, and *p*-xylene are predicted to be -38.00, -39.24, and -38.96 kcal/mol, respectively, which are greatly overestimated compared to the adsorption energies for *p*-xylene in high silica H-ZSM-5 of -19 and -27 kcal/mol reported by Rees *et al.* and Ruthven, respectively (Richards Rees, 1988; Ruthven, 1984).

To improve the calculated adsorption energies, the quantum mechanical region was extended up to 23T atoms covering all the zeolite framework atoms of the cross-section (see Figure 6, page 28). The medium layer containing 18T atoms beyond the 5T active center was added and treated quantum mechanically with the B3LYP/6-31G(d,p) level of theory. The ONIOM(MP2/6-31G(d,p):B3LYP/6-31G(d,p):UFF) adsorption energies are estimated to be -18.03, -21.16, and -21.75 kcal/mol for *o*-, *m*-, and *p*-xylene, respectively. These values are in close agreement with the experimental adsorption energy of *p*-xylene in H-ZSM-5 of -19 kcal/mol measured by gravimetric balance technique at loadings greater than 4 molecules per unit cell (Richards Rees, 1988). Although the adsorption energies of three isomers are comparable, a highly selective separation of *p*-xylene over the other isomers in H-ZSM-5 zeolite is usually reported by experiments. This can be explained by the relative molecular size of adsorbed molecules and the zeolite pore openings. Because the kinetic diameters of *o*- and *m*-xylene (6.8 Å) are larger than the pore diameter of ZSM-5 (5.8-6.0 Å), it is very difficult for these isomers to diffuse to the adsorption site (intersecting channels)

as compared to *p*-xylene with the kinetic diameter of 5.8 Å (Baertsch *et al.*, 1996; Wegner *et al.*, 1999). The experimental diffusivity of *p*-xylene in silicate (Al-free ZSM-5) has been reported to be greater than that of *o*- and *m*-xylene by a factor of 500-1000 (Roque-Malherbe *et al.*, 1995). From these results, it can be concluded that the selective separation of xylene isomer in ZSM-5 is not only controlled by the adsorption rate but also by the diffusion rate.

Chapter III: Diffusion mechanism of *p*-xylene in microporous silicalite

1. Diffusion mechanism

The trajectory plots obtained from MD simulations (see page 35) of the system at different loadings indicate that, at least at low loadings (Figure 13), the diffusion mechanism of *p*-xylene in silicalite resembles the model process of jump diffusion. The *p*-xylene molecules spend rather long periods of time at the channel intersection sites and then change rapidly to the other sites. At low temperature (300 K), most of the jumps correspond to diffusion through straight channels. Two steps can be seen from the trajectory plots. The first one is a jump from an intersection to the middle of a straight channel and the second one is the jump from the straight channel to the next intersection. Before jumping to another intersection, the molecules are localized in the straight channels for a while, indicating that the window pores of silicalite are not easy to pass by a *p*-xylene molecule. Molecular rotations are never seen during the jumps. This is due to the relative size of the *p*-xylene molecule, which is comparable to the 10 MR pore opening (Baertsch *et al.*, 1996).

Relatively few events of diffusion through sinusoidal channels can be observed at low temperature (300 K). The orientation of *p*-xylene molecules at channel intersections is likely to be parallel to the straight channel with the phenyl ring in the mid-plane between the openings of the sinusoidal pores, and the methyl groups pointing to the opening of the straight pores (see Figure 14a). To diffuse through a sinusoidal channel, the molecules have therefore to rotate by a right angle. This rotation is constricted due to the steric hindrance of the methyl groups, and so the entrance of the molecules into the sinusoidal channel is not easy.

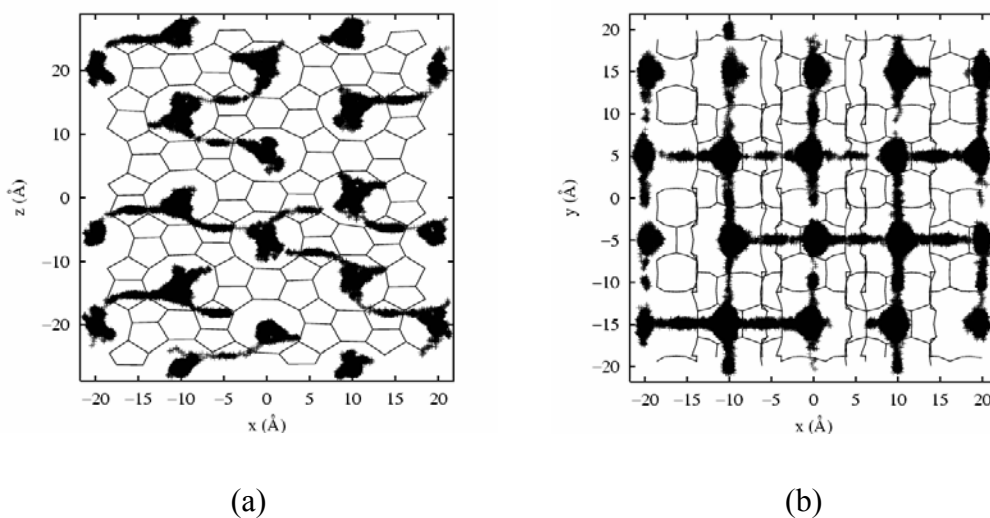


Figure 13 Guest molecule trajectories during 1 ns, from a simulation with a loading of 1 *p*-xylene per unit cell at a temperature of 500 K. The trajectory is projected onto the xy (a) and xz (b) planes.

More diffusion through the sinusoidal channel is observed when the loading is increased. This contribution becomes appreciable at the highest loading. Once the channel intersections are completely occupied, the diffusion through the straight channel is very difficult because of the strong repulsion between the methyl groups of neighboring *p*-xylene molecules. Since the molecules cannot pass each other, some molecules are forced into the sinusoidal channels (see Figure 14b). This can be seen by using graphic animation during the simulation in which molecules attempt to move through the straight channel by forcing some molecules into sinusoidal ones.

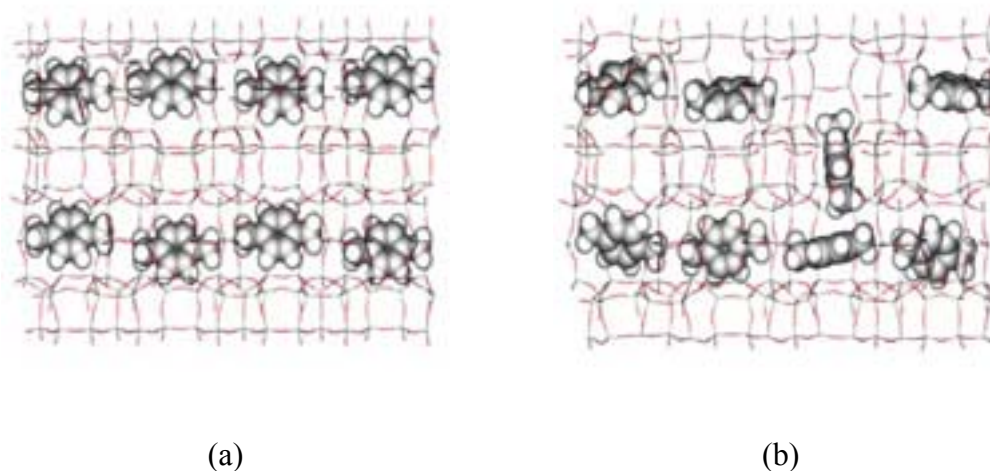


Figure 14 Molecular positions and orientations of *p*-xylene (a) before the jump and (b) during the jump in the channels of silicalite at a loading of 4 molecules per unit cell (500 K).

Figure 14 shows the jump of *p*-xylene from the channel intersection into the sinusoidal channel during the simulations at the loading of 4 molecules/unit cell. The molecular plane of *p*-xylene located at the channel intersection is oriented perpendicularly to the molecular axis of the molecule located inside the sinusoidal channel.

From this point of view, we suggest that all intersections are filled up at the loading of 4 *p*-xylene molecules/unit cell. At loadings higher than 4 molecules/unit cell, the intersections and sinusoidal channels are filled up simultaneously, while there is no occupancy in the straight channels. This is consistent with the experimental observations of Reischmann et al. (1988) and van Mentzen *et al.* (1998) that the *p*-xylene molecules begin to preferentially fill in sinusoidal channels in addition to channel intersections at loadings higher than 4 molecules/unit cell. Similar results have been obtained from MC simulations by Snurr et al. (1993).

Table 12 Self-diffusion coefficients (D) of p -xylene in silicalite at different loadings and temperatures.

loadings (molecules/unit cell)	D (cm ² /s)		
	300 K	400 K	500 K
1	1.6×10^{-7}	1.5×10^{-6}	2.8×10^{-6}
2	8.0×10^{-7}	1.6×10^{-6}	1.7×10^{-6}
3	4.2×10^{-7}	4.8×10^{-7}	1.0×10^{-6}
4	1.9×10^{-7}	4.7×10^{-7}	3.2×10^{-7}

2. Self-diffusion coefficients

The self-diffusion coefficients reported in Table 12 were obtained from the slopes at long times of the curves of the mean square displacements (MSD) of the centers of mass of the p -xylene molecules as functions of time. We note first that the calculated diffusion coefficients are of the order of 10^{-7} to 10^{-6} cm²/s, which are the same order of magnitude as found by Sastre *et al.* (1998) for p -xylene diffusion in siliceous zeolite CIT-1. These values are, however, quite larger than the experimental values (Sastre *et al.*, 1998).

The self-diffusion coefficients obtained in MD calculations may not be quantitatively comparable with experimental values. The experimental diffusion coefficients are up to 3 orders of magnitude lower (some 10^{-9} cm²/s) than those obtained in the MD simulations (Hou *et al.*, 2000; Sastre *et al.*, 1999; Sastre *et al.*, 1998). This large discrepancy could be due to the influences of the remaining aluminum in the zeolite framework as well as to the extra-framework materials, which are not included in MD simulations.

A more detailed comparison between the simulations shows that the magnitude of the values found in this work is, overall, somewhat lower than that reported by Sastre *et al.* (Sastre *et al.*, 1998). This may be due to the fact that the

diffusion of *p*-xylene in CIT-1 occurs mainly through the 12 MR channels with pore openings larger than those of the 10 MR channels of silicalite.

At the lower temperature (300 K), it is surprising that the self-diffusion coefficient is smaller for a loading of one than for a loading of 2 molecules/unit cell. At this temperature and loading, the kinetic energy is comparatively low and the distances between guest molecules are, on the average, large. Therefore the diffusivity should be mainly controlled by the *p*-xylene-zeolite interaction. This interaction becomes less important when the temperature is increased, leading to the expected temperature dependence of the self-diffusion coefficients. At higher loadings, the molecules are closer to each other, thus increasing the importance of the xylene-xylene interaction. The mutual interactions start to affect the diffusion process. The space accessible to the molecules becomes more restricted when the neighboring sites in the zeolite are also occupied. This can be clearly seen from the diffusion coefficient of the 2 molecules/unit cell system, which is faster than in the case of 3 and 4 molecules/unit cell. The diffusivity of *p*-xylene at the loading of 4 molecules/unit cell is relatively low. This is due to the channel intersections being completely occupied by *p*-xylene molecules (see above).

Chapter IV: Adsorption and diffusion of *p*-xylene in mesoporous MCM-41

1. Structure and dynamics of empty Si-MCM-41, test of force field

Before undertaking the MD simulations of the loaded systems, the initial structure of Si-MCM-41 was equilibrated for 200 ps within the NpT -ensemble to ensure that the selected structure (Figure 8, page 37) does correspond to a stable minimum of our model potential, e.g., among other things, that the simulation box does not expand or contract unreasonably. The cell dimensions after this run, $a = 39.26$ Å, $b = 22.67$ Å, and $c = 45.86$ Å are thus very close to the initial values of $a = 39.37$ Å, $b = 22.73$ Å, and $c = 45.99$ Å for the 18.6 Å pore of Gusev (Gusev). Other structural features were checked after the NpT run by computing the radial pair distribution functions of the system. The last configuration of this run was used as starting configuration for the simulations of the loaded systems (see page 36).

The infrared spectrum of Si-MCM-41 was calculated by Fourier transform of the autocorrelation function of the total dipole moment of the system using the same magnitude of the charge values used in the Si-MCM-41 model. Experimentally, the peaks observed between 500 and 1200 cm^{-1} are assigned to framework vibrations (Shanmugapriya *et al.*, 2004). In analogy with the experimental assignment, the theoretical spectrum obtained from our simple model shown in Figure 15 agrees reasonably well with the experimental data (Shanmugapriya *et al.*, 2004). The intense peak at 1089 cm^{-1} is attributed to the asymmetric stretching of the Si-O bonds. The symmetric stretching modes of these bonds are predicted at 773 cm^{-1} , and the peak at 482 and 619 cm^{-1} are due to the bending modes of Si-O-Si. These spectral features resemble those reported for highly siliceous zeolites (Smirnov *et al.*, 1993).

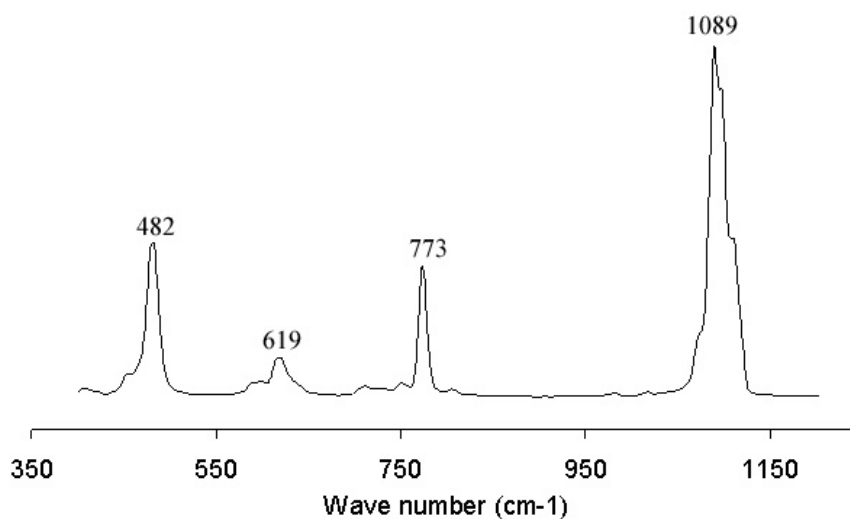


Figure 15 Simulated IR spectrum of the model Si-MCM-41.

2. Adsorption of *p*-xylene

The adsorption of aromatic hydrocarbons in the Si-MCM-41 is expected to result mainly from weak interaction of the π -electrons of the aromatic ring with the terminal silanol (Si-OH) groups (Jentys *et al.*, 1996), which are not modelled explicitly here. These interactions are included implicitly in our fitting procedure to reproduce the experimental heat of adsorption. The adsorption energies reported in Table 13 are the averages, i.e. the total guest-host interaction energies of the simulated system divided by the number of guest molecules. At our level of approximation, this energy can be identified with the heat of adsorption. We study its loading dependence and its decomposition into the van der Waals (vdW) and the Coulomb components, as shown in Table 13. The average energies were obtained from 2600 evenly spaced configurations taken after the equilibration period. At the lowest coverage that we can study ($N=1$ molecule per supercell), this energy is 11.8 kcal/mol, in good agreement with experimental heats of adsorption of 10.4 and 12.3 kcal/mol for Si-MCM-41 and H-AL-MCM-41, respectively (Choudhary and Mantri, 2000a; Choudhary *et al.*, 2000b). The former value is the one the interaction parameters were fitted to. Since *p*-xylene is a non-polar molecule, the long-range electrostatic contributions are not

expected to be significant, and we find indeed that the heat of adsorption is mainly contributed from the dispersive interactions (see Table 13.) A similar observation was made for the adsorption of benzene on the zeolite catalysts, also yielding the electrostatic contribution of only 1-2 kcal/mol (Rungsirisakun *et al.*, 2004).

Table 13 van der Waals, Coulomb, and total heats of adsorption energies and self-diffusion coefficients at different *p*-xylene loadings.

Loading Molecule(s)/supercell	Energy (kcal/mol)			<i>D</i> (cm ² /s)
	vdW	Coulomb	Total	
1	-10.0	-1.8	-11.8	-
16	-10.8	-1.9	-12.7	7.8 x 10 ⁻⁵
32	-11.3	-2.0	-13.3	5.3 x 10 ⁻⁵
48	-11.6	-2.0	-13.6	2.8 x 10 ⁻⁵
64	-11.9	-2.0	-13.9	1.8 x 10 ⁻⁵

Exploring the variation of the heat of adsorption with sorbate loading, a series of (NVE) simulations were performed on the *p*-xylene/Si-MCM-41 system, varying the number of guest molecules, *N*, as described above. Each channel was loaded with an equal number of guest molecules (except for the case of one molecule per supercell). It is found that the magnitude of adsorption energy of *p*-xylene slightly increases with increasing loading, which is similar to other hydrocarbons in narrow pore MCM-41 (Qiao *et al.*, 2004) like the one we used in this study. The loading dependence results from a balance between guest-guest and guest-host interactions. The overall trend shows that the guest-guest terms are able to overcompensate whichever less favorable guest-host interactions may arise due to mutual hindrances between guest molecules.

3. Self-diffusion of *p*-xylene

During the simulation, configurations were saved every 10 femtoseconds. The mean square displacements (MSD) of the center of mass of the *p*-xylene molecules are plotted as a function of time for different loadings in Figure 16. The self-diffusion coefficients were then determined using the Einstein relation

$$\langle X^2(t) \rangle = 6Dt + B \quad (27)$$

where $X^2(t)$ is the mean square displacement at time t , D is the self-diffusion coefficient, and B is the thermal factor arising from atomic vibrations. The self-diffusion coefficients were obtained from the slope of the curves in Figure 16. At times larger than 10 ps, the MSD is linear in time and the velocity autocorrelation function becomes zero (Figure 17), indicating that the diffusive regime has set in. The self-diffusions of *p*-xylene at different loadings are listed in Table 13. For the lowest loading ($N=1$ molecule per supercell), however, the statistics was too poor to derive a meaningful value.

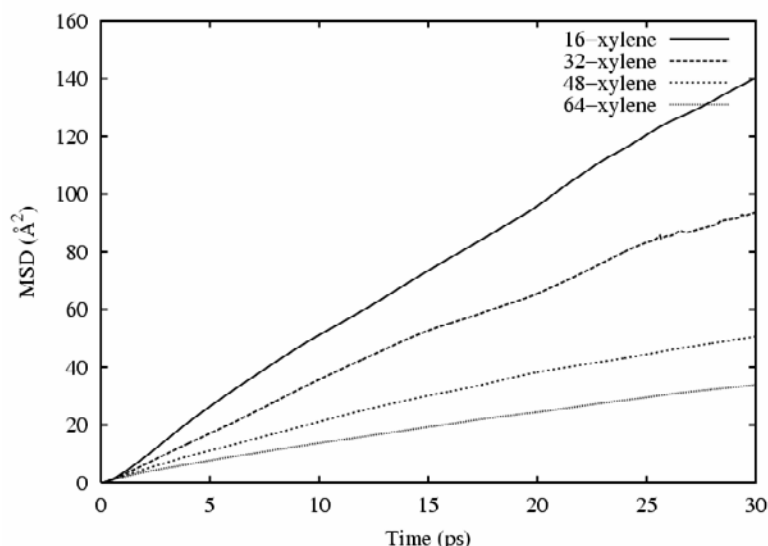


Figure 16 Mean square displacements (MSDs), at 300 K, of the centers of mass of the *p*-xylene molecules in Si-MCM-41 at different loadings.

The calculated self-diffusion coefficients decrease as loading increases. The experimental self-diffusion coefficient is not available for *p*-xylene in MCM-41. Our calculated self-diffusion coefficients are of the same order of magnitude as found in previous MD simulation for liquid *p*-xylene at 293.15 K of 1.48×10^{-5} cm²/s (Kim and Lee, 2002). Comparing to another experimental system, which is related to our study, the self-diffusion coefficients obtained from our simulations are comparable with the diffusion coefficient of pyridine in MCM-41 at 298 K (1.0×10^{-5} - 6.8×10^{-5} cm²/s) (Gedat *et al.*, 2001), even though the polarities of the two molecules are quite different.

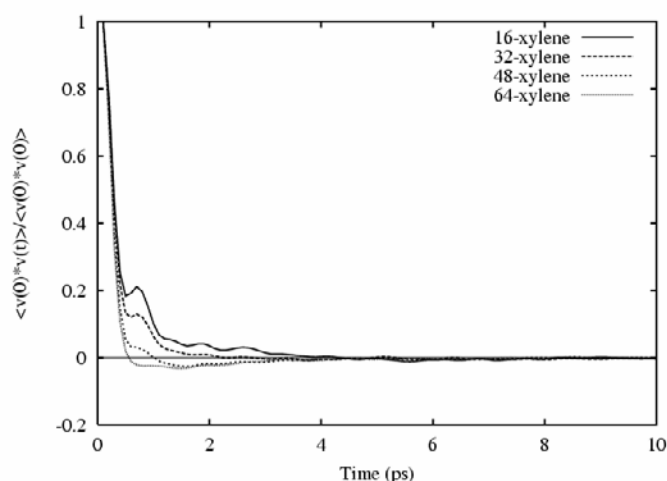


Figure 17 The normalized autocorrelation functions at 300 K of the velocity of the mass centers of the *p*-xylene molecules in Si-MCM-41 at different loadings.

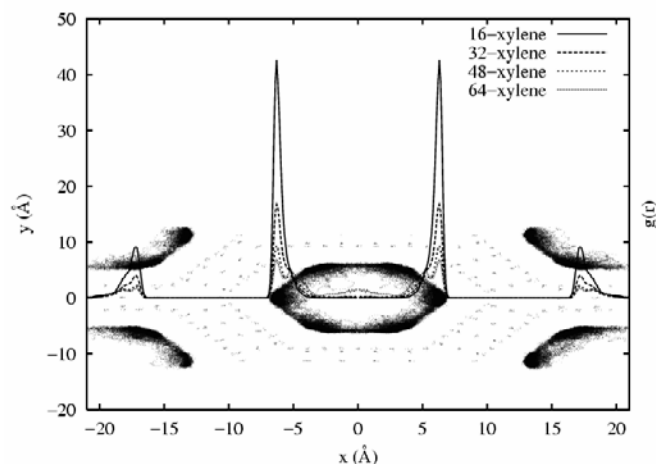


Figure 18 Projections of the trajectories of the centers of mass of *p*-xylene and the framework atoms (for 100 ps) onto the *xy*-plane at a loading of 16 molecules/supercell (black clouds and dots); cylindrical $g(r)$ distribution function of the *p*-xylene centers of mass with respect to the center of the channel for this and other loadings.

We note that the loading dependence found here is different from the one reported for pyridine in silica MCM-41 (Gedat *et al.*, 2001). Our D -values decrease by a factor of about five with increasing loading in the range studied while an increase with increasing loading is reported in (Gedat *et al.*, 2001). The two cases are, however, not directly comparable: Besides the difference in polarity already mentioned, the geometric conditions in both cases differ: In the MCM-41 studied here, the pore diameter is about 18-19 Å, while it is 33 Å for silica MCM-41. Even at the highest loading the interaction of *p*-xylene will be dominated by the guest-wall terms in the narrower pore and mutual steric hindrances will lower D . In contrast, the increased diffusivity in the wide pore is ascribed to the onset of diffusion in a second, possibly more liquid-like, layer, which fills up with increasing loading.

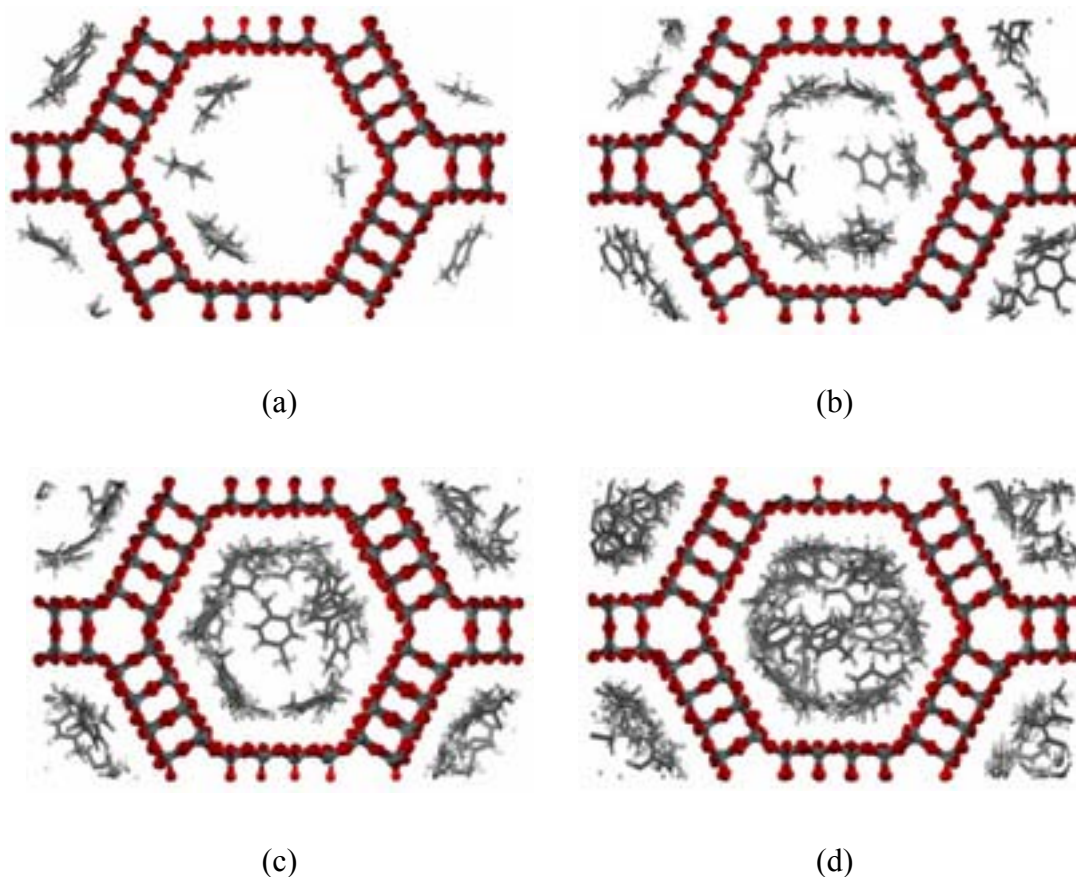


Figure 19 Snapshots of the distribution of *p*-xylene molecules in Si-MCM-41 supercell at loading of (a) 16, (b) 32, (c) 48, and (d) 64 molecules/supercell after 100 ps of MD equilibrium.

4. Radial distribution functions

Figure 18 shows the radial distribution functions of the center of mass of *p*-xylene from the channel center of MCM-41. Note that the normalization of this function is to the average density of *p*-xylene, the curve for the lowest loading thus has the largest amplitude. The single peak found at a loading of 16 molecules/supercell at about 6 Å from the center (i.e. about 3 Å from the “wall”) splits into two with increasing loading. The main peak moves to slightly closer distances to the wall and a second peak builds up at about 4 Å from the walls. The

first layer *p*-xylene molecules are thus increasingly oriented “parallel” to the wall, as seen in the snapshots of Figure. 19 a-d.

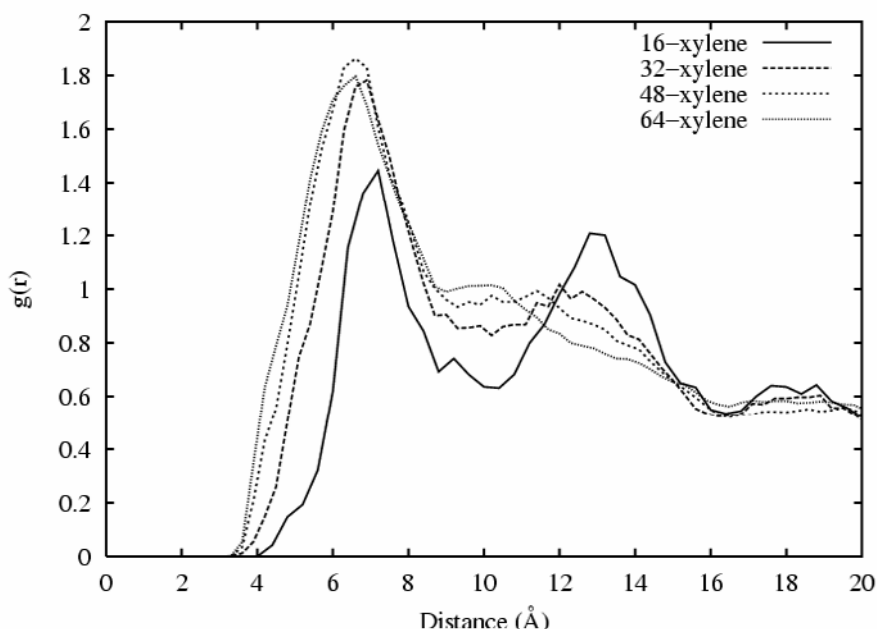


Figure 20 The center-center pair distribution functions of *p*-xylene in Si-MCM-41 at different loadings.

The center of mass pair distribution functions of *p*-xylene in MCM-41 at different loading are shown in Figure 20. We note that while the peaks broaden with increasing loading, the first maximum peak of the center-center pair distribution functions of *p*-xylene moves to slightly shorter distances to the value of about 6 Å. This value is close to the intermolecular separation in a *p*-xylene adduct derived at the B3LYP/6-31G** level of theory of 5.8 Å (see Figure. 21a). This type of configuration can be observed frequently during the diffusion of *p*-xylene in the pores (see Figure 21b). The shortest intermolecular distance during the diffusion of *p*-xylene in the pore is about 3.6 Å, which is the distance between two *p*-xylene molecules in stacked configuration. The probability of distances between this value and the peak maximum increase strongly with loading. The increasing disorder is also indicated by the disappearance of the second peak, it being shifted toward smaller distances, thus filling-up of the minimum between the two.

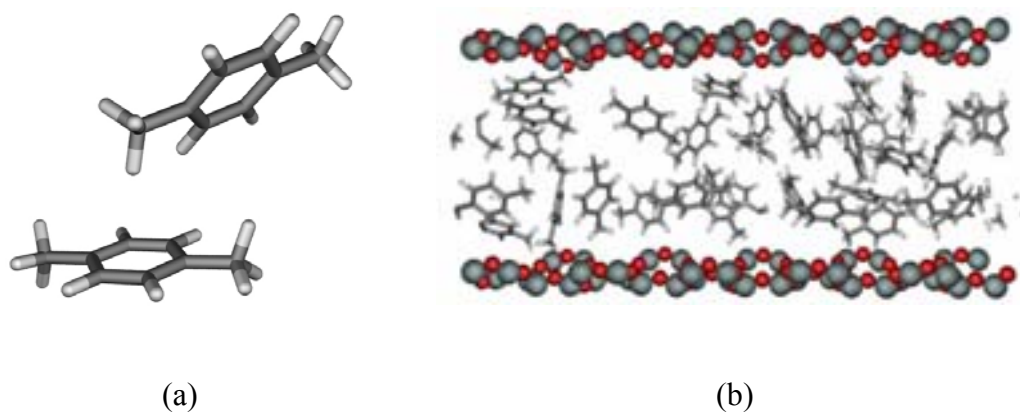


Figure 21 Illustration of (a) the configuration of *p*-xylene dimer optimized at B3LYP/6-31G(d,p) level of theory (b) a snapshot of *p*-xylene molecules in the center channel of Si-MCM-41 supercell at loading of 64 molecules/supercell after 100 ps of MD equilibrium.

CONCLUSIONS

Ethylene protonation reaction on H-FAU

Bare cluster and embedded cluster studies of the complete proton-transfer reaction mechanism of ethylene in H-FAU have been performed at density functional theory level. It was found that the 3T cluster model is too small to represent the local active site in such studies. Both the energetic and structural properties were obviously different from the 5T and 7T cluster models. However, when enlarging the active site up to 7T, the geometrical structures were insignificantly changed as compared to the 5T cluster model. This implied that, to obtain reasonable geometries, a 5T cluster model is sufficient. However, to improve the energetic properties, a single point calculation using larger cluster sizes may be necessary. The inclusion of the Madelung potential tends to enhance the ionicity of the complexes and to stabilize the ion-like transition state complex. The BSSE corrected adsorption and activation energies (-8.6 kcal/mol and 13.2 kcal/mol, respectively) calculated at the MP2/6-31G(d,p) level of theory using the 7T embedded cluster model are in good agreement with the experimental values. The reaction is exothermic by 22.57 kcal/mol, suggesting that the next step of reaction should be slow.

Shape-selective adsorption of xylene isomers in H-ZSM-5

The two-layer ONIOM scheme with the outer layer treated with the UFF force field was proven to be a reasonable model to locate the xylene isomers in the intersecting channels of the H-ZSM-5 zeolite. The energetic properties can be improved by enlarging the quantum mechanical region to cover the adsorption site. The shape of the xylene isomers was found to affect the adsorption energies. The ONIOM(MP2/6-31G(d,p):B3LYP/6-31G(d,p):UFF) single point energy calculations yield adsorption energies of -18.03 , -21.16 , and -21.75 kcal/mol for *o*-, *m*-, and *p*-xylene, respectively, comparing well with the experimental observation. The adsorption results, in combination with the diffusion studies, lead to the conclusive finding that the selective separation of xylene isomer in ZSM-5 zeolite is primarily

controlled by the diffusion rate with minor contribution due to the adsorption mechanism.

Diffusion mechanism of *p*-xylene in microporous silicalite

Dynamical properties and microscopic pictures of *p*-xylene in silicalite have been studied as a function of loading and temperature. At low loading and temperature, the diffusion of xylene molecules is primarily controlled by the zeolite-xylene interaction. This interaction, however, becomes less important when the temperature is increased, leading to the expected temperature dependence of the self-diffusion coefficients. The xylene-xylene interaction starts to affect the diffusion process when loading increases. The diffusion through sinusoidal channel becomes appreciable at higher loadings and temperatures. The detailed picture obtained from this study is in agreement with the information on the occupancy of *p*-xylene in silicalite at high loadings (more than four molecules per unit cell) and with the experimental and theoretical conclusions.

Adsorption and diffusion of *p*-xylene in Si-MCM-41

A simple model of Si-MCM-41 has been constructed and used as a mesoporous host to study the adsorption as well as the diffusion of *p*-xylene. Reasonable agreement with the available experimental data is achieved with this new force field, providing confidence to use it in order to describe the adsorption and diffusion of aromatic hydrocarbons in this material. The findings shed some light on the factors involved in the evolution of the guest-guest and guest-host interactions with increasing loading. In this model, the heat of adsorption at zero loading is due primarily to short-range van der Waals interactions between adsorbate and the walls, in keeping with chemical insight. With increasing loading, the cooperative effect of guest-guest interactions becomes more important and is able to overcompensate the less favourable guest-host interactions, thus leading to an increase of the heat of adsorption. Due to the mutual steric hindrances and the confinement effect of the narrower pore MCM-41 used in this study, the variation of the molecular self-

diffusion coefficients with loading shows the trend of decreasing with increasing loading.

LITERATURE CITED

- Alder, B. J., and T. E. Wainwright. 1957. Phase transition for a hard sphere system. **J. Chem. Phys.**, 27: 1208.
- Allouche, A. 1996a. Comparative ab Initio Study of the Chemical Reactivity of Nitromethane Adsorbed on Basic Oxides: MgO and CaO(100). **J. Phys. Chem.**, 100(5): 1820-1826.
- _____. 1996b. Quantum ab Initio Study of Acetylene Adsorption on NaCl(100). II. Excited States and Photochemistry. **J. Phys. Chem.**, 100(45): 17915-17922.
- Ashtekar, S., A. S. McLeod, M. D. Mantle, P. J. Barrie, L. F. Gladden, and J. J. Hastings. 2000. Determining the Adsorption Sites for Binary Mixtures of *p*-Xylene and n-Heptane in Silicalite Using FT-Raman Spectroscopy and Temperature-Programmed Desorption. **J. Phys. Chem. B**, 104(22): 5281-5287.
- Baertsch, C. D., H. H. Funke, J. L. Falconer, and R. D. Noble. 1996. Permeation of Aromatic Hydrocarbon Vapors through Silicalite-Zeolite Membranes. **J. Phys. Chem.**, 100(18): 7676-7679.
- Barbosa, L. A. M. M., R. A. van Santen, and J. Hafner. 2001. Stability of Zn(II) Cations in Chabazite Studied by Periodical Density Functional Theory. **J. Am. Chem. Soc.**, 123: 4530.
- Beck, J. S., J. C. Vartuli, W. J. Roth, M. E. Leonowicz, C. T. Kresge, K. D. Schmitt, C. T. W. Chu, D. H. Olson, E. W. Sheppard, S. B. McCullen, B. J. Higgins, and J. L. Schlenker. 1992. A new family of mesoporous molecular sieves prepared with liquid crystal templates. **J. Am. Chem. Soc.**, 114(27): 10834-10843.

- Bekkum, H. v., E. M. Flaningen, and J. C. e. Jansen. 1991. **Introduction to Zeolite Science and Practice**. Amsterdam: Elsevier.
- Bellat, J.-P., E. Pilverdier, M.-H. Simonot-Grange, and S. Jullian. 1997. Microporous volume and external surface of Y zeolites accessible to *p*-xylene and *m*-xylene. **Microporous Mater.**, 9(5-6): 213-220.
- _____, and M.-H. Simonot-Grange. 1995a. Adsorption of gaseous *p*-xylene and *m*-xylene on NaY, KY, and BaY zeolites. Part 2: Modeling. Enthalpies and entropies of adsorption. **Zeolites**, 15(3): 219-227.
- _____, _____, and S. Jullian. 1995b. Adsorption of gaseous *p*-xylene and *m*-xylene on NaY, KY, and BaY zeolites: Part 1. Adsorption equilibria of pure xylenes. **Zeolites**, 15(2): 124-130.
- Blaszkowski, S. R., M. A. C. Nascimento, and R. A. van Santen. 1996. Activation of C-H and C-C Bonds by an Acidic Zeolite: A Density Functional Study. **J. Phys. Chem.**, 100: 3463.
- Bobuatong, K., and J. Limtrakul. 2003. Effects of the zeolite framework on the adsorption of ethylene and benzene on alkali-exchanged zeolites: an ONIOM study. **Appl. Catal., A: General**, 253(1): 49-64.
- Boronat, M., P. Viruela, and A. Corma. 1998. Theoretical Study of the Mechanism of Zeolite-Catalyzed Isomerization Reactions of Linear Butenes. **J. Phys. Chem. A**, 102: 982-989.
- _____, C. M. Zicovich-Wilson, A. Corma, and P. Viruela. 1999. Cluster and periodic ab initio study of the ethane-ethene hydride transfer reaction catalyzed by acid chabazite. Is the cluster model able to describe accurately the host-guest interactions? **Phys. Chem. Chem. Phys.**, 1(4): 537-543.

- _____, _____, P. Viruela, and A. Corma. 2001a. Cluster and periodic calculations of ethene protonation reaction catalyzed by theta-1 zeolite. Influence of method, model size and structural constraints. **Chem. Eur. J.**, 7(6): 1295-1303.
- _____, _____, _____, and _____. 2001b. Influence of the Local Geometry of Zeolite Active Sites and Olefin Size on the Stability of Alkoxide Intermediates. **J. Phys. Chem. B**, 105(45): 11169-11177.
- Boys, S. F., and F. Bernardi. 1970. Counterpoise correction for the basis set superposition error (BSSE). **Mol. Phys.**, 19: 553.
- Brandle, M., J. Sauer, R. Dovesi, and N. M. Harrison. 1998. Comparison of a combined quantum mechanics/interatomic potential function approach with its periodic quantum-mechanical limit: Proton siting and ammonia adsorption in zeolite chabazite. **J. Chem. Phys.**, 109(23): 10379-10389.
- Breneman, C. M., and K. B. Wiberg. 1990. Determining atom-centered monopoles from molecular electrostatic potentials. The need for high sampling density in formamide conformational analysis. **J. Comp. Chem.**, 11: 361-373.
- Cant, N. W., and W. K. Hall. 1972. Studies of the hydrogen held by solids : XXI. The interaction between ethylene and hydroxyl groups of a Y-zeolite at elevated temperatures. **J. Catal.**, 25: 161.
- Cao, D., Z. Shen, J. Chen, and X. Zhang. 2004. Experiment, molecular simulation and density functional theory for investigation of fluid confined in MCM-41. **Microporous Mesoporous Mater.**, 67: 159-166.
- Catlow, C. R. A., C. M. Freeman, B. Vessal, S. M. Tomlinson, and M. Leslie. 1991. Molecular dynamics studies of hydrocarbon diffusion in zeolites. **J. Chem. Soc. Faraday Trans.**, 87(13): 1947-1950.

- Chenite, A., Y. L. Page, and A. Sayari. 1995. Direct TEM Imaging of Tubules in Calcined MCM-41 Type Mesoporous Materials. **Chem. Mater.**, 7: 1015.
- Choudhary, V. R., P. Devadas, S. Banerjee, and A. K. Kinage. 2001. Aromatization of dilute ethylene over Ga-modified ZSM-5 type zeolite catalysts. **Microporous Mesoporous Mater.**, 47: 253.
- _____, and K. Mantri. 1998. Temperature-Programmed Desorption of Benzene on Mesoporous Si-MCM-41, Na-ALSi-MCM-41, and H-ALSi-MCM-41. **Langmuir**, 16(21): 8024-8030.
- _____, and _____. 2000a. Adsorption of Aromatic Hydrocarbons on Highly Siliceous MCM-41. **Langmuir**, 16(17): 7031-7037.
- _____, and _____. 2000b. Temperature programmed desorption of toluene, *p*-xylene, mesitylene and naphthalene on mesoporous high silica MCM-41 for characterizing its surface properties and measuring heats of adsorption. **Microporous Mesoporous Mater.**, 40: 127-133.
- _____, D. Panjala, and S. Banerjee. 2002. Aromatization of propene and n-butene over H-galloaluminosilicate (ZSM-5 type) zeolite. **Appl. Catal. A: Gen.**, 231: 243.
- Clark, L. A., M. Sierka, and J. Sauer. 2002. Relative stability of alkoxides and carbocations in zeolites. QM/MM embedding and QM calculations applying periodic boundary conditions. **Stud. Surf. Sci. Catal.**, 142A(Impact of Zeolites and Other Porous Materials on the New Technologies at the Beginning of the New Millennium): 643-649.

- Climent, M. J., A. Corma, S. Iborra, M. C. Navarro, and J. Primo. 1996. Use of Mesoporous MCM-41 Aluminosilicates as Catalysts in the Production of Fine Chemicals: Preparation of Dimethylacetals. **J. Catal.**, 161: 783-789.
- Corma, A., and A. V. Orchilles. 2000. Current views on the mechanism of catalytic cracking. **Microporous Mesoporous Mater.**, 35-36: 21-30.
- Cornell, W. D., P. Cieplak, C. I. Bayly, I. R. Gould, K. M. Merz, D. M. Ferguson, D. C. Spellmeyer, T. Fox, J. W. Caldwell, and P. A. Kollman. 1995. A second generation force field for the simulation of proteins, nucleic acids, and organic molecules. **J. Am. Chem. Soc.**, 117: 5179.
- Correa, R. J., and C. J. A. Mota. 2002. Theoretical study of protonation of butene isomers on acidic zeolite: the relative stability among primary, secondary and tertiary alkoxy intermediates. **Phys. Chem. Chem. Phys.**, 4(2): 375.
- Costa Vaya, V. I., P. G. Belelli, J. H. Z. dos Santos, M. L. Ferreira, and D. E. Damiani. 2001. Influence of Acidic Support in Metallocene Catalysts for Ethylene Polymerization. **J. Catal.**, 204: 1-10.
- Deka, R. C., and K. Hirao. 2002. Lewis acidity and basicity of cation-exchanged zeolites: QM/MM and density functional studies. **J. Mol. Catal. A: Chem.**, 181(1-2): 275-282.
- Dwyer, J. 1991. Synthesis, Structure and Reactivity. In E. G. Derouane, F. Lemos, C. Naccache, and F. R. Ribeiro (Eds.), **Zeolite Microporous Solids**: 303. London: Kluwer Academic Publ.
- Ermoshin, V. A., K. S. Smirnov, and D. Bougeard. 1996. Ab initio generalized valence force field for zeolite modelling. 1. Siliceous zeolites. **Chem. Phys.**, 202: 53-61.

- Evleth, E. M., E. Kassab, H. Jessri, M. Allavena, L. Montero, and L. R. Sierra. 1996. Calculation of the Reaction of Ethylene, Propene, and Acetylene on Zeolite Models. **J. Phys. Chem.**, 100: 11368.
- Ferrari, A. M., and G. Pacchioni. 1996. Metal Deposition on Oxide Surfaces: A Quantum-Chemical Study of the Interaction of Rb, Pd, and Ag Atoms with the Surface Vacancies of MgO. **J. Phys. Chem.**, 100(21): 9032-9037.
- Ferro, Y., A. Allouche, F. Cora, C. Pisani, and C. Girardet. 1995. Adsorption of NH₃ on MgO(100): a comparative study of ab initio and semi-classical calculations. **Surf. Sci.**, 325: 139.
- Feuston, B. P., and J. B. Higgins. 1992. Model Structures for MCM-41 Materials: A Molecular Dynamics Simulation. **J. Phys. Chem.**, 98(16): 4459-4462.
- Frash, M. V., V. B. Kazansky, A. M. Rigby, and R. A. van Santen. 1998. Cracking of Hydrocarbons on Zeolite Catalysts: Density Functional and Hartree-Fock Calculations on the Mechanism of the β -Scission Reaction. **J. Phys. Chem. B.**, 102: 2232.
- Gedat, E., A. Schreiber, G.H. Findenegg, I. Shenderovich, H.-H. Limbach, and G. Buntkowsky 2001. Stray Field Gradient NMR Reveals Effects of Hydrogen Bonding on Diffusion Coefficients of Pyridine in Mesoporous Silica. **Magn. Reson. Chem.**, 39: S149-S157.
- Girgis, M. J., and Y. P. Tsao. 1996. Impact of Catalyst Metal-Acid Balance in n-Hexadecane Hydroisomerization and Hydrocracking. **Ind. Eng. Chem. Res.**, 35(2): 386-396.

- Guo, G.-Q., H. Chen, and Y.-C. Long. 2000. Separation of *p*-xylene from C8 aromatics on binder-free hydrophobic adsorbent of MFI zeolite. I. Studies on static equilibrium. **Microporous Mesoporous Mater.**, 39(1-2): 149-161.
- Gusev, V. <http://boba.boom.ru/eng/mcm-41.html>.
- Ha, V. T. T., L. V. Tiep, P. Meriaudeau, and C. Naccache. 2002. Aromatization of methane over zeolite supported molybdenum: active sites and reaction mechanism. **J. Mol. Catal. A: Chem.**, 181: 283.
- Hill, J.-R., C. M. Freeman, and B. Delley. 1999. Bridging Hydroxyl Groups in Faujasite: Periodic vs Cluster Density Functional Calculations. **J. Phys. Chem. A**, 103(19): 3772-3777.
- Hillier, I. H. 1999. Chemical reactivity studied by hybrid QM/MM methods. **J. Mol. Struct.: THEOCHEM**, 463(1-2): 45-52.
- Hou, T. J., L. L. Zhu, and X. J. Xu. 2000. Adsorption and Diffusion of Benzene in ITQ-1 Type Zeolite: Grand Canonical Monte Carlo and Molecular Dynamics Simulation Study. **J. Phys. Chem. B**, 104(39): 9356-9364.
- Ivanov, P., and H. Papp. 2000. FT-IR Study of the Isomerization of n-Butene over Different Zeolites. **Langmuir**, 16(20): 7769-7772.
- Jentys, A., N. H. Pham, and H. Vinek. 1996. The nature of hydroxyl groups in MCM-41. **J. Chem. Soc. Faraday Trans.**, 92(17): 3287.
- Jiang, N., S. Yuan, J. Wang, Z. Qin, H. Jiao, and Y.-W. Li. 2005. An ONIOM study of amines adsorption in H-[Ga]MOR. **J. Mol. Catal. A: Chem.**, 232(1-2): 59-67.

- Joshi, Y. V., and K. T. Thomson. 2005. Embedded cluster (QM/MM) investigation of C₆ diene cyclization in HZSM-5. **J. Catal.**, 230(2): 440-463.
- Kärger, J., S. Vasenkov, and S. M. Auerbach. 2003. **Handbook of Zeolite Science and Technology**. In S. M. Auerbach, K. A. Carrado, and P. K. Dutta (Eds.): 341-422: Marcel Dekker, Inc.
- Kasuriya, S., S. Namuangruk, P. Treesukol, M. Tirtowidjojo, and J. Limtrakul. 2003. Adsorption of ethylene, benzene, and ethylbenzene over faujasite zeolites investigated by the ONIOM method. **J. Catal.**, 219(2): 320-328.
- Katada, N., T. Tsubouchi, M. Niwa, and Y. Murakami. 1995. Vapor-phase Beckmann rearrangement over silica monolayers prepared by chemical vapor deposition. **Appl. Catal. A**, 124(1): 1-7.
- Kazanskii, V. B. 1991a. The nature of adsorbed carbenium ions as active intermediates in catalysis by solid acids. **Acc. Chem. Res.**, 24(12): 379-383.
- _____. 1991b. The nature of adsorbed carbenium ions as active intermediates in catalysis by solid acids. **Acc. Chem. Res.**, 24: 379.
- _____. 1999. Adsorbed carbocations as transition states in heterogeneous acid catalyzed transformations of hydrocarbons. **Catal. Today**, 51: 419.
- _____. 2002. Solvation as a main factor that determines the strength of liquid superacids and the selectivity of the acid-catalyzed reactions of olefins. **Catal. Today**, 73: 127.
- Ketrat, S., and J. Limtrakul. 2003. Theoretical study of the adsorption of ethylene on alkali-exchanged zeolites. **Int. J. Quantum Chem.**, 94(6): 333-340.

- Kim, J. H., and S. H. Lee. 2002. Molecular Dynamics Simulation Studies of Benzene, Toluene, and *p*-Xylene in NpT Ensemble: Thermodynamic, Structural, and Dynamic Properties. **Bull. Korean. Chem. Soc.**, 23: 447.
- Klamt, A., and G. Schuurmann. 1993. 'COSMO: a new approach to dielectric screening in solvents with explicit expressions for the screening energy and its gradient. **J. Chem. Soc. Perkin Trans.**, 2: 799-805.
- Kleestorfer, K., H. Vinek, and A. Jenty. 2001. Structure simulation of MCM-41 type materials. **J. Mol. Catal. A: Chem.**, 166: 53-57.
- Kondo, J. N., K. Domen, and F. Wakabayashi. 1998. Double bond migration of 1-butene without protonated intermediate on D-ZSM-5. **Microporous Mesoporous Mater.**, 21: 429.
- Koningsveld, H. v. 1990. High-temperature (350 K) orthorhombic framework structure of zeolite H-ZSM-5. **Acta Cryst.**, B46: 731-735.
- Larin, A. V., D. N. Trubnikov, and D. P. Vercauteren. 2005. Improvement of X-ray diffraction geometries of water physisorbed in zeolites on the basis of periodic hartree-fock calculations. **Int. J. Quantum Chem.**, 102(5): 971-979.
- Limtrakul, J., S. Jungsuttiwong, and P. Khongpracha. 2000a. Adsorption of carbon monoxide on H-FAU and Li-FAU zeolites. An embedded cluster approach. **J. Mol. Struct.**, 525: 153-162.
- _____, P. Khongpracha, S. Jungsuttiwong, and T. N. Truong. 2000b. Adsorption of carbon monoxide in H-ZSM-5 and Li-ZSM-5 zeolites. An embedded ab initio cluster study. **J. Mol. Catal. A: Chem.**, 153(1-2): 155-163.
- _____, T. Nanok, S. Jungsuttiwong, P. Khongpracha, and T. N. Truong. 2001. Adsorption of unsaturated hydrocarbons on zeolites: the effects of the zeolite

- framework on adsorption properties of ethylene. **Chem. Phys. Lett.**, 349(1,2): 161-166.
- Maddox, M. W., J. P. Olivier, and K. E. Gubbins. 1997. Characterization of MCM-41 Using Molecular Simulation: Heterogeneity Effects. **Langmuir**, 13(6): 1737-1745.
- Martinez-Magadan, J. M., A. Cuan, and M. Castro. 2002. An embedded QM/MM study for different SiO₂/Al₂O₃ ratios of the HZSM-5 zeolite and for their interaction with N-heptane. **Int. J. Quantum Chem.**, 88(6): 750-766.
- Mentzen, B. F., and P. Gelin. 1998. Location of *p*-Xylene and Cesium Cations in ZSM-5 and Cs-ZSM-5: Structural Evidence for the Formation of a [π]-Complex. **Mater. Res. Bull.**, 33(1): 109-116.
- Mickael, P., M. Francesco, and J. P. Chris. 2003. Accurate First Principles Prediction of ¹⁷O NMR Parameters in SiO₂: Assignment of the Zeolite Ferrierite Spectrum. **J. Am. Chem. Soc.**, 125: 543.
- Mohanty, S., H. T. Davis, and A. V. McCormick. 2000. Shape selective adsorption in atomistic nanopores -- a study of xylene isomers in silicalite. **Chem. Eng. Sci.**, 55(15): 2779-2792.
- _____, and A. V. McCormick. 1999. Prospects for principles of size and shape selective separations using zeolites. **Chem. Eng. J.**, 74: 1.
- Mortier, W. J., E. van den Bossche, and J. B. Uytterhoeven. 1984. Influence of the temperature and water adsorption on the cation location in NaY zeolites. **Zeolites**, 4: 41-44.

- Nair, S., and M. Tsapatsis. 2000. The Location of *o*- and *m*-Xylene in Silicalite by Powder X-ray Diffraction. **J. Phys. Chem. B**, 104(38): 8982-8988.
- Namba, S., J.-H. Kim, T. Komatsu, and T. Yashima. 1997. Novel purification method of commercial *o*- and *m*-xylenes by shape selective adsorption on HZSM-5. **Microporous Mater.**, 8(1-2): 39-42.
- Namuangruk, S., P. Pantu, and J. Limtrakul. 2004. Alkylation of benzene with ethylene over faujasite zeolite investigated by the ONIOM method. **J. Catal.**, 225(2): 523-530.
- Nguyen, C., C. G. Sonwane, S. K. Bhatia, and D. D. Do. 1998. Adsorption of Benzene and Ethanol on MCM-41 Material. **Langmuir**, 14(17): 4950-4952.
- Nicholas, J. B., and A. C. Hess. 1994. Ab Initio Periodic Hartree-Fock Investigation of a Zeolite Acid Site. **J. Am. Chem. Soc.**, 116(12): 5428-5436.
- _____, A. J. Hopfinger, F. R. Trouw, and L. E. Iton. 1991. Molecular modeling of zeolite structure. 2. Structure and dynamics of silica sodalite and silicate force field. **J. Am. Chem. Soc.**, 113: 4792.
- Niessen, W., and H. G. Karge. 1993. Diffusion of *p*-xylene in single and binary systems in zeolites investigated by FTIR spectroscopy. **Microporous Mater.**, 1(1): 1-8.
- O'Malley, P. J., and K. J. Farnworth. 1998. Density Functional Studies of Weak Base Interactions with Hydroxyl Groups: Models for Adsorption Complexes of Weak Bases in Microporous Materials. **J. Phys. Chem. B**, 102: 4507.

- Panjan, W., and J. Limtrakul. 2003. The influence of the framework on adsorption properties of ethylene/H-ZSM-5 system: an ONIOM study. **J. Mol. Struct.**, 654(1-3): 35-45.
- Qiao, S. Z., S. K. Bhatia, and D. Nicholson. 2004. Study of Hexane Adsorption in Nanoporous MCM-41 Silica. **Langmuir**, 20(2): 389-395.
- Raksakoon, C., and J. Limtrakul. 2003. Adsorption of aromatic hydrocarbon onto H-ZSM-5 zeolite investigated by ONIOM study. **THEOCHEM**, 631: 147-156.
- Ravikovitch, P. I., C. O. SDomhnaill, A. V. Neimark, F. Schueth, and K. K Unger. 1995. Capillary Hysteresis in Nanopores: Theoretical and Experimental Studies of Nitrogen Adsorption on MCM-41. **Langmuir**, 11(12): 4765-4772.
- _____, D. Wei, W. T. Chueh, G. L. Haller, and A. V. Neimark. 1997. Evaluation of Pore Structure Parameters of MCM-41 Catalyst Supports and Catalysts by Means of Nitrogen and Argon Adsorption. **J. Phys. Chem. B**, 101(19): 3671-3679.
- Reischman, P. T., K. D. Schmitt, and D. H. Olson. 1988. A theoretical and NMR study of *p*-xylene sorption into ZSM-5. **J. Phys. Chem.**, 92(18): 5165-5169.
- Richards, R. E., and L. V. C. Rees. 1988. The sorption of *p*-xylene in ZSM-5. **Zeolites**, 8(1): 35-39.
- Roque-Malherbe, R., R. Wendelbo, A. Mifsud, and A. Corma. 1995. Diffusion of aromatic hydrocarbons in H-ZSM-5, H-Beta, and H-MCM-22 zeolites. **J. Phys. Chem.**, 99(38): 14064-14071.
- Rozanska, X., T. Demuth, F. Hutschka, J. Hafner, and R. A. van Santen. 2002a. A Periodic Structure Density Functional Theory Study of Propylene

Chemisorption in Acidic Chabazite: Effect of Zeolite Structure Relaxation. **J. Phys. Chem. B**, 106(12): 3248-3254.

_____, R. A. van Santen, and F. Hutschka. 2002b. A Periodic Density Functional Theory Study of Intermolecular Isomerization of Toluene and Benzene Catalyzed by Acidic Mordenite Zeolite: Effect of the Zeolite Steric Constraints. **J. Phys. Chem. B**, 106(18): 4652-4657.

_____, _____, _____, and J. Hafner. 2001. A Periodic DFT Study of Intramolecular Isomerization Reactions of Toluene and Xylenes Catalyzed by Acidic Mordenite. **J. Am. Chem. Soc.**, 123(31): 7655-7667.

_____, _____, _____, and _____. 2002c. A Periodic DFT Study of the Isomerization of Thiophenic Derivatives Catalyzed by Acidic Mordenite. **J. Catal.**, 205(2): 388-397.

Rungsirisakun, R., B. Jansang, P. Pantu, and J. Limtrakul. 2004. The adsorption of benzene on industrially important nanostructured catalysts (H-BEA, H-ZSM-5, and H-FAU): confinement effects. **J. Mol. Struct.**, 733(1-3): 239-246.

Ruthven, M. D. 1984. **Principles of Adsorption and Adsorption Processes**. New York: John Wiley.

Sakai, H., T. Tomita, and T. Takahashi. 2001. *p*-Xylene separation with MFI-type zeolite membrane. **Sep. Pur. Tech.**, 25(1-3): 297-306.

Sastre, G., C. R. A. Catlow, and A. Corma. 1999. Diffusion of Benzene and Propylene in MCM-22 Zeolite. A Molecular Dynamics Study. **J. Phys. Chem. B**, 103(25): 5187-5196.

- Sastre, G., N. Raj, C. R. A. Catlow, R. Roque-Malherbe, and A. Corma. 1998. Selective Diffusion of C8 Aromatics in a 10 and 12 MR Zeolite. A Molecular Dynamics Study. **J. Phys. Chem. B**, 102(17): 3198-3209.
- Schrimpf, G., M. Schlenkrich, J. Brickmann, and P. Bopp. 1992. Molecular dynamics simulation of zeolite NaY: a study of structure, dynamics, and thermalization of sorbates. **J. Phys. Chem.**, 96: 7404-7410.
- Schwarz, K., E. Nusterer, and P. E. Blochl. 1997. First-principle molecular dynamics study of small molecules in zeolites. **Preprints - Am. Chem. Soc., Div. Petr. Chem.**, 42(1): 69-75.
- Shah, R., J. D. Gale, and M. C. Payne. 1996. Methanol Adsorption in Zeolites - A First-Principles Study. **J. Phys. Chem.**, 100(28): 11688-11697.
- _____, _____, and _____. 1997. In Situ Study of Reactive Intermediates of Methanol in Zeolites from First Principles Calculations. **J. Phys. Chem. B**, 101(24): 4787-4797.
- Shanmugapriya, K., M. Palanichamy, B. Arabindoo, and V. Murugesan. 2004. A novel route to produce thymol by vapor phase reaction of *m*-cresol with isopropyl acetate over Al-MCM-41 molecular sieves. **J. Catal.**, 224: 347-357.
- Sherwood, P., A. H. de Vries, M. F. Guest, G. Schreckenbach, C. R. A. Catlow, S. A. French, A. A. Sokol, S. T. Bromley, W. Thiel, and A. J. Turner. 2003. QUASI: A general purpose implementation of the QM/MM approach and its application to problems in catalysis. **J. Mol. Struct.: THEOCHEM**, 632(1-3): 1-28.
- Shor, E. A. I., A. M. Shor, V. A. Nasluzov, G. N. Vayssilov, and N. Roesch. 2005. Effects of the Aluminum Content of a Zeolite Framework: A DFT/MM

- Hybrid Approach Based on Cluster Models Embedded in an Elastic Polarizable Environment. **J. Chem. Theory Comp.**, 1(3): 459-471.
- Sillar, K., and P. Burk. 2004. Hybrid Quantum Chemical and Density Functional Theory (ONIOM) Study of the Acid Sites in Zeolite ZSM-5. **J. Phys. Chem. B**, 108(28): 9893-9899.
- Smirnov, K. S., and D. Bougeard. 1993. Molecular dynamics study of the vibrational spectra of siliceous zeolites built from sodalite cages. **J. Phys. Chem.**, 97: 9434.
- Snurr, R. Q., A. T. Bell, and D. N. Theodorou. 1993. Prediction of adsorption of aromatic hydrocarbons in silicalite from grand canonical Monte Carlo simulations with biased insertions. **J. Phys. Chem.**, 97(51): 13742-13137.
- Sonwane, C. G., and Q. Li. 2005. Structure and Transport Properties of Nanostructured Materials. **J. Phys. Chem. B**, 109(12): 5691-5699.
- Stefanovich, E. V., and T. N. Truong. 1998. A Simple Method for Incorporating Madelung Field Effects into ab Initio Embedded Cluster Calculations of Crystals and Macromolecules. **J. Phys. Chem. B**, 102(16): 3018-3022.
- Svensson, M., S. Humbel, R. D. J. Froese, T. Matsubara, S. Sieber, and K. Morokuma. 1996. ONIOM: A Multilayered Integrated MO + MM Method for Geometry Optimizations and Single Point Energy Predictions. A Test for Diels-Alder Reactions and Pt(P(t-Bu)₃)₂ + H₂ Oxidative Addition. **J. Phys. Chem.**, 100: 19357-19363.
- Treesukol, P., J. P. Lewis, J. Limtrakul, and T. N. Truong. 2001a. A full quantum embedded cluster study of proton siting in chabazite. **Chem. Phys. Lett.**, 350(1,2): 128-134.

- _____, J. Limtrakul, and T. N. Truong. 2001b. Adsorption of nitrogen monoxide and carbon monoxide on copper-exchanged ZSM-5. A cluster and embedded cluster study. **J. Phys. Chem. B**, 105(12): 2421-2428.
- Trombetta, M., A. G. Alejandre, J. R. Solis, and G. Busca. 2000. An FT-IR study of the reactivity of hydrocarbons on the acid sites of HZSM5 zeolite. **Appl. Catal. A: Gen.**, 198(1-2): 81-93.
- Ugliengo, P., A. M. Ferrari, A. Zecchina, and E. Garrone. 1996. Structure and Vibrational Features of Complexes between Unsaturated Hydrocarbons and Acidic Sites in Silica and Zeolites: An ab Initio Study. **J. Phys. Chem.**, 100: 3632.
- Verlet, L. 1967. Computer "experiment" on classical fluids. I. Thermodynamical properties of Lennard-Jones molecules. **Phys. Rev.**, 159: 98-103.
- Viruela-Martin, P., C. M. Zicovich-Wilson, and A. Corma. 1993. Ab initio molecular orbital calculations of the protonation of propylene and isobutene by acidic hydroxyl groups of isomorphously substituted zeolites. **J. Phys. Chem.**, 97: 3713.
- Vollmer, J. M., E. V. Stefanovich, and T. N. Truong. 1999. Molecular Modeling of Interactions in Zeolites: An Ab Initio Embedded Cluster Study of NH₃ Adsorption in Chabazite. **J. Phys. Chem. B**, 103(44): 9415-9422.
- _____, and T. N. Truong. 2000. Mechanisms of Hydrogen Exchange of Methane with H-Zeolite Y: An ab Initio Embedded Cluster Study. **J. of P. Chem. B**, 104(26): 6308-6312.
- Vos, A. M., K. H. L. Nulens, F. De Proft, R. A. Schoonheydt, and P. Geerlings. 2002. Reactivity Descriptors and Rate Constants for Electrophilic Aromatic

Substitution: Acid Zeolite Catalyzed Methylation of Benzene and Toluene. **J. Phys. Chem. B**, 106(8): 2026-2034.

_____, X. Rozanska, R. A. Schoonheydt, R. A. van Santen, F. Hutschka, and J. Hafner. 2001. A Theoretical Study of the Alkylation Reaction of Toluene with Methanol Catalyzed by Acidic Mordenite. **J. Am. Chem. Soc.**, 123(12): 2799-2809.

Wegner, K., J. Dong, and Y. S. Lin. 1999. Polycrystalline MFI zeolite membranes: xylene pervaporation and its implication on membrane microstructure. **J. Membr. Sci.**, 158: 17-27.

Zhao, X. S., G. Q. Lu, and G. J. Millar. 1996. Advances in Mesoporous Molecular Sieve MCM-41. **Ind. Eng. Chem. Res.**, 35(7): 2075-2090.

Zygmunt, S. A., L. A. Curtiss, P. Zapol, and L. E. Iton. 2000. Ab Initio and Density Functional Study of the Activation Barrier for Ethane Cracking in Cluster Models of Zeolite H-ZSM-5. **J. Phys. Chem. B**, 104: 1944.

CURRICULUM VITAE

NAME : Mr. Tanin Nanok

BIRTH DATE : August 18, 1977

BIRTH PLACE : Nakornratchasima, Thailand

NATIONALITY : Thai

EDUCATION : YEAR INSTITUTION DEGREE/DIPLOMA

2000 Kasetsart University B.Sc. (Chemistry)

SCHOLASHIP : The Thailand Research Fund Royal Golden Jubilee Ph.
D. Program

Higher Education Development Project Scholarship
Postgraduate Education and Research Program in
Physical Chemistry (2000-2005)

Teaching Assistance, Physical Chemistry Division,
Kasetsart University (2000-2001)

The Kasetsart University Research and Development
Institute (KURDI)

PUBLICATIONS

1. Limtrakul, J., T. Nanok, S. Jungsuttiwong, P. Khongpracha, T. N. Truong. 2001. Adsorption of unsaturated hydrocarbons on zeolites: The effects of the zeolite framework on adsorption properties of ethylene. **Chem. Phys. Lett.**, 349: 161-166.
2. Nanok, T., P. A. Bopp, J. Limtrakul. 2005. Diffusion mechanism of *p*-xylene in nanoporous silicalite: A molecular dynamics simulation study. **Preprints-**

American Chemical Society, Division of Petroleum Chemistry, 50: 231-234.

3. Nanok, T., P. A. Bopp, J. Limtrakul. Molecular dynamics simulation studies of *p*-xylene in OH-free Si-MCM-41. submitted.
4. Nanok, T., P. A. Bopp, J. Limtrakul. Shape-selective adsorption of xylene isomers in H-ZSM-5: An ONIOM study. to be submitted.

PRESENTATIONS

1. Nanok, T. and J. Limtrakul. 2001. Potential energy surface of ethylene reaction on zeolite: The embedded quantum cluster study. **27th Congress in Science and Technology of Thailand**, Song-Khla, Thailand, October 16-18, 2001.
2. Nanok, T. and J. Limtrakul. 2002. The effects of the crystal framework on mechanism of ethylene reaction with FAU catalyst: Cluster and density functional theory. **233rd ACS National Meeting & Exposition**, Orlando, FL, United States, April 7-11, 2002.
3. Nanok, T, P. A. Bopp, J. Limtrakul. 2004. Molecular dynamics simulations of the self-diffusion of *p*-xylene in silicalite. **30th Congress in Science and Technology of Thailand**, Bangkok, Thailand, October 19-21, 2004.
4. Nanok T, P. A. Bopp, J.Limtrakul.2005 Diffusion mechanism of *p*-xylene in nanoporous silicalite: A molecular dynamics simulation study. **229th ACS National Meeting & Exposition**, San Diego, CA, United States, March 13-17, 2005.